Global Scale Mapping of Subsurface Scattering Signals Impacting ASCAT Soil Moisture Retrievals

CITATION

DOI

Global Scale Mapping of Subsurface Scattering Signals Impacting ASCAT Soil Moisture Retrievals

Wolfgang Wagner, *Senior Member, IEEE,* Roland Lindorfer, Sebastian Hahn, Hyunglok Kim,
Mariette Vreugdenhil, Alexander Gruber, Milan Fischer, and Miroslav Trnka

Abstract—Soil moisture retrievals from the Advanced Scatterometer (ASCAT) have so far relied on the assumption that soil backscatter increases monotonically with soil moisture content. However, under dry soil conditions, discontinuities in the soil profile caused by the presence of stones, rocks or distinct soil layers may disturb this relation, causing backscatter to decrease with increasing soil wetness. As of yet, subsurface scattering is a poorly understood phenomenon and some of its manifestations on ASCAT soil moisture retrievals have in the past been wrongly attributed to topographic effects or changes in soil surface roughness and vegetation. Therefore, this study aims at mapping subsurface scattering effects on a global scale, explore their dependency on land surface characteristics, and describe the impacts on ASCAT soil moisture retrievals. The results obtained with one statistical and two physically based indicators show that subsurface scattering is not only widespread in desert regions, but also in more humid climates with a dry season. Along with the dryness of the soil, the presence of coarse fragments in the soil profile and sparse vegetation cover are important factors that favor its occurrence. The impact on ASCAT soil moisture retrievals is severe, making subsurface scattering the main error source in the current version of the ASCAT soil moisture data as provided by the EUMETSAT Satellite Application Facility on Support to Operational Hydrology and Water Management. Users of the product are recommended to mask soil moisture data affected by subsurface scattering effects using the indicators and masks developed in this study.

Index Terms—Radar remote sensing, C-band, land surface, soil moisture, soil properties.

I. INTRODUCTION

THE Advanced Scatterometer (ASCAT) is an active microwave remote sensing instrument that has been flown on a series of three Metop satellites operated by the European Organization for the Exploitation of Meteorological Satellites (EUMETSAT) [1]. It measures the backscattering coefficient at a frequency of 5.255 GHz (C-band) which, over land, is sensitive to the water content in the soil surface layer. This allows retrieving surface soil moisture (SSM) data using statistical and physically based approaches [2]–[5]. ASCAT SSM

W. Wagner is with the Department of Geodesy and Geoinformation, Technische Universität Wien, 1040 Vienna, Austria, and part time with the EODC and – at the time of writing – with the Global Change Research Institute of the Czech Academy of Sciences (e-mail: wolfgang.wagner@geo.tuwien.ac.at).

R. Lindorfer, S. Hahn, M. Vreugdenhil and A. Gruber are with the Department of Geodesy and Geoinformation, Technische Universität Wien, 1040 Vienna, Austria.

H. Kim is with the School of Earth Sciences and Environmental Engineering, Gwangju Institute of Science and Technology, Gwangju 61005, Republic of Korea

M. Fischer and M. Trnka are with the Global Change Research Institute of the Czech Academy of Sciences

Manuscript received XXX; revised XXX

data retrieved using the change detection algorithm developed by TU Wien [6] are available from the EUMETSAT Satellite Application Facility on Support to Operational Hydrology and Water Management (H SAF) [6]. The data serve numerous applications such as numerical weather prediction, rainfall estimation, and flood and drought monitoring [7]. In many ways the H SAF ASCAT SSM data are similar to SSM data provided by the L-band Soil Moisture Active Passive (SMAP) and Soil Moisture Ocean Salinity (SMOS) missions, and higher-frequency radiometers such as the Advanced Microwave Scanning Radiometer 2 (AMSR2) [8]–[11]. Therefore it is possible to fuse them with passive SSM data to create consistent climate data records that are more accurate than single satellite data records [12], [13]. The prerequisite to achieve such an improvement is a detailed understanding of the accuracy of each input data set and a fusion technique capable of optimally merging the individual satellite data records [14].

As is best practice in the validation of satellite soil moisture retrievals [15], [16], the ASCAT SSM data have been assessed in numerous validation studies [17]–[21] using multiple independent reference data sets, including in situ data as available from the International Soil Moisture Network (ISMN) [22], modeled soil moisture data from the fifth generation of European ReAnalysis (ERA5) [23] and Global Land Data Assimilation System [24], and passive SSM data sets from SMOS, SMAP or AMSR2. Validation methods ranged from calculating standard performance metrics such as time series correlation and unbiased root mean square error [25], [26], to more advanced techniques such as triple collocation [27], instrumental variable regression [28] or Fourier analysis [29].

Many of these validation studies specifically addressed the question of how the quality of the ASCAT SSM retrievals depends on land cover and vegetation [18], [20], [21], [30]. Given that vegetation dampens the signals from the soil surface, the expectation is that the uncertainty of ASCAT SSM retrievals increases with increasing biomass in a similar way as for passive soil moisture retrievals. However, contrary to this expectation, ASCAT SSM data have been found to be of better quality over grasslands and agricultural regions than over bare or sparsely vegetated regions [8], [31]. In many arid and semi-arid environments, ASCAT SSM data are even negatively correlated with in situ and modeled soil moisture data.

Wagner et al. [6] hypothesized that the retrieval errors observed in arid regions may be caused by the high penetration of C-band waves into dry soil, leading to volume scattering from stony soil layers or scattering by subsurface discontinuities, e.g., a rock surface beneath a shallow layer of sand. This explanation was supported by controlled laboratory experiments with a C-band profiling radar that allows resolving signals originating from the soil surface layer from subsurface signals [32]. These experiments demonstrated that a distinct, brightly reflecting subsurface below a 10–12 cm thick layer of sand can produce strong backscatter signals, causing total backscatter to increase when the moisture content of the sand decreases. This behavior can be modeled with an exponential subsurface scattering term that predicts an increase of subsurface scattering contributions with decreasing soil wetness that may counteract the signal from the soil surface [33]. When confronting the bare soil backscatter model with and without the new subsurface scattering term to three years of ASCAT backscatter observations acquired over a region covering parts of south-western Europe and north-western Africa, it was found that subsurface scattering is not just limited to arid environments, but appears to be a much more widespread phenomenon that may also emerge in more humid regions during dry periods [33].

For ASCAT SSM retrievals, it would hence be essential to account not only for the scattering contributions from the soil surface and vegetation layers but also for those from subsurface discontinuities. Unfortunately, this is currently not the case in the TU Wien change detection algorithm, impairing the quality of the H SAF ASCAT SSM data. To varying degrees, this also affects downstream soil moisture data products such as produced by the European Space Agency's Climate Change Initiative (ESA CCI) [34], the Copernicus Global Land Monitoring Service (CGLS) [35], [36] and the National Oceanic and Atmospheric Administration [13].

Therefore, this study aims at detecting subsurface scattering effects at a global scale and discussing their impacts on ASCAT SSM retrievals. This will contribute to the understanding of the interaction of C-band microwaves with the Earth's surface and allow users of H SAF ASCAT SSM data to make informed decisions about where and when to mask the SSM retrievals. Additionally, the subsurface scattering information obtained from this study can serve as a crucial and independent predictor, alongside other factors such as vegetation and soil properties, in the development of more accurate models for predicting uncertainties in remotely sensed soil moisture datasets [12], [37].

This paper is structured as follows: In Sec. II we provide a theoretical discussion of the different types of errors in the ASCAT SSM retrievals that may occur in case of subsurface scattering. After describing all data used in this study (Sec. III), the methods for detecting subsurface scattering effects are presented in Sec. IV. The results shown in Sec. V reveal a strong dependency of subsurface scattering effects on climate, soil and vegetation properties. The usefulness of the derived subsurface scattering maps for masking ASCAT SSM retrievals is discussed in Sec. VI, followed by the conclusions in Sec. VII.

II. THEORY

The H SAF ASCAT SSM retrieval scheme is based on the TU Wien change detection model originally developed for the ERS scatterometer [38], and later adapted to ASCAT [2], [39], [40]. This backscatter model is formulated in the decibel domain, assuming that a change in soil moisture leads to a change in backscatter

$$\Delta\sigma^0[\text{dB}] = S\Delta\theta \tag{1}$$

where θ is the soil moisture content in degree of saturation, σ^0 the backscattering coefficient expressed in dB, and S is the sensitivity of σ^0 to θ. This linear relationship is assumed to hold over the entire incidence angle range of ASCAT ($25°$ to $65°$) for bare soils and vegetated covered ground alike.

To obtain estimates of θ, the model is calibrated for each land surface pixel by extracting minimum and maximum backscatter values from multi-year backscatter time series standardized to a reference angle of $40°$ and corrected for seasonal vegetation cover effects [40]–[42]. The so-derived values of σ^0_{min} and σ^0_{max} do not only vary from pixel to pixel, but also over the seasons and are assumed to represent completely dry and saturated soil conditions, respectively. Furthermore, assuming stable land cover and soil surface roughness, the backscattering coefficient σ^0 as measured by ASCAT and other spaceborne radar sensors is then written as

$$\sigma^0[\text{dB}] = \sigma^0_{min} + S \cdot \theta \tag{2}$$

with $S = \sigma^0_{max} - \sigma^0_{min}$. Like σ^0_{min} and σ^0_{max}, the sensitivity S varies in space and time, reflecting the patterns of land cover and vegetation phenology. By inverting Eq. 2, soil moisture can be obtained

$$\theta_A(t) = \frac{\sigma^0(t) - \sigma^0_{min}}{S} \tag{3}$$

where t is the time of acquisition. The subscript A indicates that this is an estimate of the area-averaged soil moisture content based on ASCAT.

Functionally, the way how the TU Wien change detection model describes the backscatter behavior of vegetation is similar to the Water Cloud model introduced by Attema and Ulaby [43] to simulate backscatter from agricultural fields. The Water Cloud model is essentially a zeroth-order radiative transfer solution for the vegetation canopy that can be combined with different soil backscatter models. Using an exponential bare soil backscatter model, the Water Cloud model can be written in a simplified form [33]

$$\sigma^0[\text{m}^2\text{m}^{-2}] = \sigma^0_{veg} + \Gamma^2_{veg}\alpha e^{\beta\theta} \tag{4}$$

where σ^0 is the backscattering coefficient as given in Eq. 2 (but this time in linear scale), σ^0_{veg} is the volume scattering contribution from the vegetation canopy, Γ^2_{veg} is the two-way attenuation factor describing the two-way loss of energy through the vegetation, α is the surface scattering contribution when the soil is dry ($\theta = 0$), and β describes the sensitivity of bare soil backscatter to soil moisture changes.

For naturally occurring values of σ^0 in the range 0.01 to 10 m^{2}m^{-2} both the TU Wien change detection model (Eq. 2) and the Water Cloud model (Eq. 4) resemble second-order polynomial functions between σ^0 and θ, and predict, under all circumstances, an increase of σ^0 when the soil surface becomes wetter. Both models are hence unable to describe subsurface scattering effects that cause backscatter to increase when the soil dries. In the case of the Water Cloud model, this deficiency can be resolved by introducing an exponential subsurface scattering term of the form $\psi e^{-\xi\theta}$, where ψ is the scattering coefficient of the subsurface scatterers (such as bedrock or stones covered by a layer of sand) and ξ regulates the strength of the attenuation of the subsurface scattering signals by the intermediate soil layer [33]. With this additional term, the backscattering coefficient of vegetation-covered soil (with subsurface scatterers) becomes

$$\sigma^0[\text{m}^2\text{m}^{-2}] = \sigma^0_{veg} + \hat{\alpha}e^{\beta\theta} + \hat{\psi}e^{-\xi\theta} \qquad (5)$$

where $\hat{\alpha}$ and $\hat{\psi}$ are the surface and subsurface scattering coefficients dampened by the vegetation layer, i.e. $\hat{\alpha} = \Gamma^2_{veg}\alpha$ and $\hat{\psi} = \Gamma^2_{veg}\psi$. Note that vegetation phenology causes σ^0_{veg} and Γ^2_{veg} to vary over the year particularly at high incidence angles where the path of the microwaves through the vegetation canopy is larger. At low incidence angles, seasonal changes due to vegetation are smaller. Therefore, following [33], we assume that at an incidence angle of $20°$ the three model parameters σ^0_{veg}, $\hat{\alpha}$ and $\hat{\psi}$ can in a first approximation be treated as constants. This allows focusing on the effects caused by subsurface scatterers as discussed in the following.

Eq. 5 shows that, depending on the relative strengths of the surface and subsurface terms, σ^0 either increases or decreases with increasing soil wetness. This leads to three functionally different backscatter regimes: (i) dominant surface scattering, (ii) dominant subsurface scattering, (iii) and mixed scatter regime. These regimes are illustrated by Fig. 1 which furthermore serves to discuss the expected impacts on ASCAT SSM retrievals.

< Fig. 1 >

Let us start from the worst possible case from the point of view of the current TU Wien algorithm, i.e., dominant subsurface scattering (Fig. 1a). In this scenario, subsurface scattering is very strong under all weather conditions, resulting in an inverted monotonic relationship between σ^0 and θ (Fig. 1a). In principle, this could enable the derivation of reliable soil moisture estimates from the ASCAT measurements. The primary distinction from a "regular" retrieval would be that the physical mechanism causing the backscatter response to changes in soil moisture is not the enhanced scattering contribution from the soil surface but the damping of the subsurface scattering signals with increasing θ. Regardless, with the current TU Wien algorithm this scenario leads to physically meaningless SSM estimates that are negatively correlated with true soil moisture values. It was exactly this kind of behavior observed in spaceborne radar observations over desert regions [6], [44]–[46] that has prompted this line of research.

In the mixed scattering scenario illustrated by Fig. 1b, the subsurface scattering signals are weaker than in the first scenario, but still sufficiently strong to cause an initial decline of σ^0 with increasing wetness, leading to a U-shaped relationship between σ^0 and θ. This is a challenging scenario for any type of soil moisture retrieval scheme, given that there is no unique mapping of a σ^0 measurement to one SSM value. Potentially, this ambiguity might be resolved by using additional observations (e.g., other polarizations, frequencies, etc.) or other ancillary data sets capable of signaling the occurrence of subsurface scattering [32]. For the current TU Wien algorithm, the impact of this scenario is also quite severe in that the ASCAT SSM retrievals are meaningful only for wet soil conditions, while during dry periods "anomalies" occur. Depending on the strength of the subsurface scatters and climatic conditions, these anomalies may occur each year during the dry season or only intermittently in exceptionally dry periods [41], [47]. This might lead to counter-intuitive situations where the ASCAT SSM data indicate a wetting of the soil while an ongoing drought intensifies.

In the last scenario (Fig. 1c) subsurface scattering is either weak or non-existent, not changing the monotonic relationship between σ^0 and θ. Therefore, the ASCAT SSM retrievals should not show irregularities due to subsurface scattering. However, the additional scattering energy may reduce the sensitivity of σ^0 to changes in θ for dry soil conditions. Therefore, H SAF ASCAT SSM retrievals may vary little when the soils dry, while in situ soil or modeled soil moisture data still continue to decrease [33]. Interestingly, this effect may, to some extent, be compensated by backscatter saturation effects for wet conditions as predicted by many bare soil backscatter models [48], including the widely used Integral Equation Model [49] or the semi-empirical Dubois model [50].

III. Data

ASCAT backscatter and SSM data were processed for the years 2007 to 2021 at a global scale and compared to climate reanalysis data from ERA5-Land, in situ data from the ISMN, and various ancillary data sets characterizing climatic conditions and soil and vegetation properties. A selection of key reference data sets is shown in Fig. 2: three thematic maps showing climate classes, land cover, and soil groups, and three maps showing continuous land surface variables, namely mean relative soil moisture, leaf area index (LAI), and the volumetric fraction of coarse fragments (CFVO) in the 5-15 cm soil layer. The ASCAT, ERA5-Land and ISMN data are described in more detail in the following subsections, while all other data sets are briefly summarized in Table I.

< Fig. 2 >

< Table I >

A. ASCAT Backscatter and Soil Moisture

ASCAT is a fan beam scatterometer that captures backscatter triplets in VV polarization along two 550 km wide swaths. The three antennas on each side are oriented at $45°$, $90°$, and $135°$ with respect to the satellite track [1], viewing the

Earth's surface at incidence angles ranging from $34°$ to $65°$ for the fore and aft beams, and from $25°$ to $55°$ for the mid beam. Because of this multiple-viewing capability, it is possible to determine the slope and curvature that characterize the backscatter – incidence angle relationship. This, in turn, allows for correcting seasonal vegetation effects in the soil moisture retrievals [40] and extrapolating the ASCAT backscatter triplets to any desired reference angle [51]. To minimize seasonal vegetation effects in our procedures to detect subsurface scattering, we computed ASCAT backscatter data at a reference angle of $20°$ [33].

To build the ASCAT backscatter and SSM time series for the years 2007 and 2021, we extracted all the necessary data fields from the H SAF data records H119 and H120 [52] which comprise data from the three Metop satellites: Metop-A (2006–2021), Metop-B (launch 2012) and Metop-C (launch 2018). The data come with a spatial resolution of about 25 km and are sampled on a fixed Earth grid with 12.5 km sampling distance and 838,275 land pixels.

We masked the ASCAT data in regions where a soil moisture retrieval is not possible for physical reasons: (i) Dense tropical forest areas were masked based on ASCAT confidence flags (bits 4 and 5) as well as LAI data (LAI > 3) from CGLS. (ii) Open water bodies and seasonally flooded wetland areas were masked using the Global Lakes and Wetlands Database [53] together with land cover information (classes 160, 170 and 180) and the ASCAT confidence flag bit 3. (iii) Snow and frost conditions were also masked using the confidence flag supplied by the H SAF record (bit 1) in combination with ERA5-Land soil temperature ($\leq 2\,°C$) and snow depth data (> 0 mm after averaging with a sliding window of 31 days) as masking criteria.

B. ERA5-Land Soil Moisture

ERA5-Land is a global dataset for the land component of the fifth generation of European ReAnalysis (ERA5) implemented by the European Centre for Medium-Range Weather Forecasts (ECMWF) [23]. It combines model data with observations and describes the evolution of the water and energy cycles over land by means of meteorological forcing from the ERA5 climate reanalysis and the Carbon Hydrology-Tiled ECMWF Scheme for Surface Exchanges over Land (CHT-ESSEL) model. Key updates of the CHTESSEL land surface model include a revised soil hydrology, the introduction of a climatological seasonality of vegetation as well as a new scheme for bare soil evaporation. Soil moisture and other land surface variables are derived on a 9 km grid with an hourly temporal sampling [54]. Importantly, ERA5-Land and ASCAT are independent since ERA5-Land does not assimilate land surface observations, in contrast to ERA5. Modeled soil moisture data are taken from the ERA5-Land's volumetric soil water layer 1 ranging from 0 to 7 cm. The hourly data record from 2007 to 2021 was resampled to the global 12.5 km grid used for ASCAT and temporally collocated to match the time stamps of the ASCAT measurements. The ERA5-Land soil moisture data were then scaled between the minimum and maximum values from 2007–2021 for each pixel to achieve a

relative indicator θ_E, ranging from 0 to 100 % such as θ_A. Frost and snow masking was carried out as for ASCAT. Fig. 2b shows the mean θ_E values after applying the snow and frost mask.

C. ISMN Soil Moisture

Data from the International Soil Moisture Network (ISMN) are used to evaluate results obtained from the analysis using the ERA5-Land data. The ISMN serves as a centralized data hosting facility with globally available in situ soil moisture measurements from operational networks and validation campaigns [22]. The network contains data from more than 70 networks with over 2,800 stations. For this study we selected stations that acquired measurements over the complete study period from 2007 to 2021. All available records of SSM (0–10 cm) in this time span were matched with the spatially and temporally nearest ASCAT measurements. As for θ_A and θ_E, ISMN soil moisture was scaled to retrieve a relative index θ_I. ISMN data flags [55] were used for masking frozen soil and snow conditions in combination with ASCAT and ERA5-Land flags to achieve an equivalent masking procedure. Unfortunately, spatial coverage is extremely uneven across the globe, with the bulk of the data coming from the contiguous United States and comparably few or even no data from the other continental regions (see Table II).

< Table II >

IV. METHODS

To detect subsurface scattering signals we look for their 'fingerprints' in ASCAT backscatter data as discussed in Sec. II; that is, we aim to detect instances where backscatter increases (rather than decreases) when the soil dries. We limit the analysis to areas where ASCAT is sensitive to signals from the ground surface for most of the year, i.e. cold regions, water bodies, wetlands, and tropical forest areas are disregarded. We note that this is important to reduce the number of spurious signals picked up by the methods as described below.

Building upon the algorithms introduced by Wagner et al. [33] we use here three indicators of subsurface scattering, namely the probability of the occurrence of backscatter anomalies, $\mathcal{P}_{ano}$, the probability of detecting subsurface scattering, $\mathcal{P}_{sub}$, and the subsurface scattering signal strength, $\mathcal{S}_{sub}$. All three indicators are calculated from ASCAT $\sigma^0(20)$ time series collocated to either modeled (ERA5-Land) or in situ (i.e., ISMN) soil moisture data.

The first indicator, $\mathcal{P}_{ano}$, is a simple but powerful statistical indicator of subsurface scattering. It depicts how frequently the ASCAT backscatter data exhibit anomalies (i.e., strong negative correlations with a reference soil moisture data set) over a given region and time frame. It is calculated by firstly computing the Spearman rank correlation ρ between $\sigma^0(20)$ and θ_E or θ_I for each day of the complete data record using a sliding window of one month (31 days). Then, the number of days N when ρ is smaller than -0.4 is computed and compared with the total number of days, N_{total}, within

the considered time frame. This yields an estimate of the probability of the occurrence of backscatter anomalies

$$\mathcal{P}_{ano} = \frac{N\left(\rho < -0.4\right)}{N_{total}} \quad (6)$$

The time frame can in principle be chosen arbitrarily, but should not be too short to yield statistically meaningful results. In this study, $\mathcal{P}_{ano}$ was computed over all years (2007–2021) and for each month (all years).

The idea behind this indicator is illustrated in Fig. 3 which shows a backscatter time series from the Sahel zone in Mali. The observed behavior is quite typical for regions in Africa with distinct wet and dry seasons [56]–[59]: During the wet season, which lasts in this region from about July to October, ASCAT backscatter closely follows the reference soil moisture time series and ρ is strongly positive. However, in the dry season, backscatter gradually increases in the absence of rainfall. Given that at the same time ERA5-Land shows a subtle decrease in soil moisture, the rank correlation may fall below the -0.4 threshold. Also note the decrease in backscatter at the onset of the 2012 rainfall season after the first few rainfall events, which brings backscatter down to the lowest point of the U-shaped curve, as shown in Fig. 1b.

< Fig. 3 >

The other two indicators, $\mathcal{P}_{sub}$ and $\mathcal{S}_{sub}$, are derived using a physically based method that compares the goodness of fit of two backscatter models — one without ($\mathcal{M}_0$) and one with ($\mathcal{M}_1$) the subsurface scattering term [33]. By replacing σ_{veg}^0 in Eq. 5 with a generic constant backscatter term, c_σ, that accounts not only for vegetation but also other types of land cover (urban areas, rocks, etc.), these two models are written

$$\begin{aligned} \mathcal{M}_0 : \sigma^0 &= c_\sigma + \hat{\alpha}e^{\beta\theta} \\ \mathcal{M}_1 : \sigma^0 &= c_\sigma + \hat{\alpha}e^{\beta\theta} + \hat{\psi}e^{-\xi\theta} \end{aligned} \quad (7)$$

Following [33] we fitted the two models to three-year data subsets and selected the best model using k-fold cross-validation for each subset. Soil moisture (θ) is either from ERA5-Land (θ_E) or ISMN (θ_I). In case of very similar model performance $\mathcal{M}_0$ is preferred over $\mathcal{M}_1$. The data subsets were formed by using a sliding time window $[Y-1, Y+1]$ for all years Y within the period from 2008 to 2020. Using these 13 data subsets, we calculated the probability of detecting subsurface scattering with

$$\mathcal{P}_{sub} = \frac{N\left(\mathcal{M}_1\right)}{N\left(\mathcal{M}_0\right) + N\left(\mathcal{M}_1\right)} \quad (8)$$

where $N\left(\mathcal{M}_1\right)$ is the number of subsets for which $\mathcal{M}_1$ was selected, and $N\left(\mathcal{M}_0\right)$ is the corresponding number of subsets for which no subsurface scattering term was needed to explain the observations, i.e. where $\mathcal{M}_0$ sufficed to explain the variability in the data.

Finally, the strength of the subsurface scattering signal $\mathcal{S}_{sub}$ was calculated from the model parameters $\hat{\psi}$ and ξ that were estimated when fitting the model $\mathcal{M}_1$ to each subset of data. It is defined as the signal range of the subsurface scattering term $\hat{\psi}e^{-\xi\theta}$ from completely dry ($\theta = 0\%$) to wet ($\theta = 100\%$) conditions

$$\mathcal{S}_{sub} = \hat{\psi}\left(1 - e^{-\xi}\right) \quad (9)$$

It is given in linear units (m^2 m^{-2}). Here we use its median value over all 13 subsets. Note that we also tested alternative time frames (e.g. for each month over all years) to compute $\mathcal{P}_{sub}$ and $\mathcal{S}_{sub}$. However, results (not shown) either became unstable if the data subset was too small or were not significantly different from the results presented here.

V. RESULTS

We calculated the three subsurface scattering indicators $\mathcal{P}_{ano}$, $\mathcal{P}_{sub}$ and $\mathcal{S}_{sub}$ using θ_E and θ_I independently of each other. As the maps for the contiguous United States (Fig. 4) show, the indicators based on the point-like ISMN data exhibit more spatial variability than the maps based on the coarse-scale reanalysis data. Nonetheless, the large-scale patterns agree reasonably well: subsurface scattering signals are detected particularly in the arid southwest while they are mostly absent in the humid eastern parts of the region. The spatial correlation between the ERA5-Land and ISMN based indicators is 0.65 for $\mathcal{P}_{ano}$, 0.20 for $\mathcal{P}_{sub}$ and 0.22 for $\mathcal{S}_{sub}$. While this is a quite good result for $\mathcal{P}_{ano}$, the values are relatively low for $\mathcal{P}_{sub}$ and $\mathcal{S}_{sub}$.

< Fig. 4 >

The differences between $\mathcal{P}_{ano}$ on the one hand, and $\mathcal{P}_{sub}$ and $\mathcal{S}_{sub}$ on the other, are particularly apparent when having a closer look at the results over the eastern part of the CONUS area. While $\mathcal{P}_{ano}$ is consistently low for both ERA5-Land and ISMN, $\mathcal{P}_{sub}$ and $\mathcal{S}_{sub}$ have several outlier values over ISMN stations. Furthermore, $\mathcal{P}_{sub}$ and $\mathcal{S}_{sub}$ depict strong signals in the colder and wetter northeast for ERA5-Land. As these signals are strongest near the fringes of our snow and frost mask and near wetlands/lakes, we attribute this latter effect to the presence of surface water and wet snow that can cause a decrease of backscatter for wet conditions. This favors the (wrongful) selection of $\mathcal{M}_1$ over $\mathcal{M}_0$ (Eq. 7) as only $\mathcal{M}_1$ is able to simulate a decrease of backscatter with increasing wetness conditions.

This behavior observed over the CONUS area is also apparent in the three global indicator maps based upon ERA5-Land shown in Fig. 5: Apart from spurious effects in colder regions and around wetlands, the three global indicator maps exhibit the expected behavior at large, depicting subsurface scattering predominantly in arid and semi-arid regions with no or low vegetation cover and poor soils with coarse fragments. To quantify the dependence of the three indicators on climate, land cover and soil classes, we calculated for each class c the fraction of pixels (stations) for ERA5-Land (ISMN) for which each indicator exceeds a certain threshold set to exclude noise

$$f_c = \frac{N\left(\text{indicator} > \text{threshold}\right)}{N_c} \quad (10)$$

where N_c is the total number of pixels or stations within a given class c. The noise thresholds were set to 0.1 (10%) for both $\mathcal{P}_{ano}$ and $\mathcal{P}_{sub}$, and 0.005 m^2 m^{-2} for $\mathcal{S}_{sub}$.

< Fig. 5 >

Table III shows f_c values (in %) for the Köppen-Geiger climate classification, ISRIC soil groups, and the ESA CCI land cover classification. To ease the interpretation of the table, f_c values larger than 30 % and the corresponding classes are highlighted by bold type setting. By and large, the results from the three indicators based on either the ERA5-Land or ISMN data are consistent with each other. Nonetheless, one can see that the $\mathcal{P}_{ano}$ results show a more distinct relationship to the different classification schemes than do the results for $\mathcal{P}_{sub}$, and, even more so, $\mathcal{S}_{sub}$. Moreover, the class separability is better for f_c values based on the ERA5-Land data than on ISMN. In line with our observations from above, this suggests that one needs to be cautious when interpreting $\mathcal{P}_{sub}$ and $\mathcal{S}_{sub}$, particularly when based on ISMN data and over higher latitude/altitude regions with seasonal snow cover and water bodies.

Considering these caveats, the conclusions that can be drawn from Table III are that subsurface scattering is primarily observed in the arid climate zone (B-climates), continental climates with dry summers (Ds), and the hot-summer Mediterranean climate (CSa). In line with this dependence on climatic conditions, bare land and soils with sparse vegetation/herbaceous cover, grassland, and shrubland are particularly prone to subsurface scattering. Soil groups that favor subsurface scattering are Arenosols (unconsolidated sand deposits), Calcisols ('desert' soils), Cambisols (a soil in the beginning of soil formation), Gypsisols (soils in semi-arid regions with the accumulation of gypsum in the subsurface), Leptosols (very shallow soil over hard rock or a deeper soil that is extremely gravelly or stony), Regosols (weakly developed mineral soil in unconsolidated materials) and Solonchaks (pale or grey soil type found in arid to subhumid poorly-drained conditions).

< Table III >

For the comparison to continuous land surface fields, we computed spatial correlations between the three indicators and five variables that can be expected to influence subsurface scattering effects in either a rather direct manner (i.e., mean soil moisture, CFVO, sand fraction) or indirectly (i.e., LAI, terrain). As Table IV shows, ISMN results are again less clear but nonetheless corroborate the dependencies as depicted by the ERA5-Land results (mostly for $\mathcal{P}_{ano}$). As expected, the mean soil moisture conditions in an area represent the most important direct control of subsurface scattering effects, with rank correlations ranging between -0.4 and -0.8 for the three ERA-Land based indicators. The correlations are also very good for LAI, which implies that the mean LAI reflects critical soil properties (moisture, structure) well.

< Table IV >

Quite surprising are the results for the fractions of coarse fragments and sand in the soil. While the sand fraction seems to be a poor diagnostic variable at the scale of our analysis, CFVO is found to be a much better predictor. As illustrated by Fig. 6, all three indicators consistently increase with CFVO

for both ERA5-Land and ISMN data. The increase is most gradual for $\mathcal{P}_{ano}$ and most pronounced for $\mathcal{S}_{sub}$ which takes on non-zero larger values only for CFVO values in the highest quarter of the distribution (from about 180 to 320 cm^3 dm^{-3}). Last but not least, elevation is only a weak predictor but one can nonetheless note that some of the strongest subsurface scattering signals are found in arid mountain ranges.

< Fig. 6 >

Let us now address the different sensitivities exhibited by the three indicators seen in all results so far. While $\mathcal{P}_{ano}$ picks up signals over a broader range of environmental conditions, $\mathcal{P}_{sub}$ and even more so $\mathcal{S}_{sub}$ are more confined to arid regions and show much more pronounced spatial patterns. This may indicate that, comparable to the overestimation problem of $\mathcal{P}_{sub}$ and $\mathcal{S}_{sub}$ in cold and wetland regions, also $\mathcal{P}_{ano}$ is sensitive to other physical effects that cause subsurface-scattering-like signals. However, when plotting $\mathcal{P}_{ano}$ for individual months one finds that it follows the succession of dry and wet seasons extremely well, with high values during the dry season and values at or near zero during the wet season. This behavior can be nicely observed over Africa (Fig. 7) where $\mathcal{P}_{ano}$ behaves anti-cyclic to the movement of the intertropical convergence zone (ITCZ). As the ITCZ, which is a major control on tropical rainfall [60], reaches its northernmost position in July–August, soils across the whole Sahelian belt have become sufficiently wet to switch off subsurface scattering. The same is true in southern Africa when the ITCZ reaches its southernmost position in January–February. Quite remarkable is the widespread occurrence of subsurface scattering signals during the dry season in both the Sahel and southern Africa. These high $\mathcal{P}_{ano}$ values are caused by the backscatter behavior seen in long dry seasons as already discussed for the backscatter time series from Mali (see Fig. 3).

< Fig. 7 >

VI. DISCUSSION

The results show that, broadly speaking, the spatial patterns depicted by the three subsurface scattering indicators $\mathcal{P}_{ano}$, $\mathcal{P}_{sub}$ and $\mathcal{S}_{sub}$ reflect the global distribution of climate, land cover and soil types quite well (cf Fig. 1). Furthermore, all three exhibit the expected dependencies on soil moisture, soil properties (CFVO) and (indirectly) vegetation (LAI). This gives us confidence that all three indicators do a reasonable job in picking up subsurface scattering signals. Nonetheless, it is also clear that they may both over- and underestimate the extent of subsurface scattering areas. Unfortunately, at the global level and the spatial scale observed by ASCAT, independent field observations do not exist, which means that it is impossible to compute a confusion matrix and associated metrics such as the classification accuracy. Alternatively, we evaluate the usefulness of three indicators by their ability to mask out inaccurate ASCAT retrievals. But before doing so, let us discuss possible reasons for both over- and under-detection.

Considering that $\mathcal{P}_{ano}$ covers much larger areas than $\mathcal{P}_{sub}$ and $\mathcal{S}_{sub}$, one may be tempted to assume that $\mathcal{P}_{ano}$ has a stronger tendency than $\mathcal{P}_{sub}$ and $\mathcal{S}_{sub}$ to over-detect subsurface

scattering areas by picking up other anomalous backscatter signals. However, when carefully analyzing Fig. 5, one can note that, also on a global level, $\mathcal{P}_{sub}$ and $\mathcal{S}_{sub}$ depict more erratic signals near wetlands and cold regions than $\mathcal{P}_{ano}$ does. Furthermore, as we have already seen for Africa (cf. Fig. 7 and Fig. 3) the weaker signals picked up by $\mathcal{P}_{ano}$ look plausible, occurring predominately during the dry seasons. So even though there may of course be isolated short-term anomalies accidentally caused by noise in the backscatter measurements or due to physical effects such as seasonal flooding, there is no evidence to assume that over-detection is a bigger problem for $\mathcal{P}_{ano}$ than it is for $\mathcal{P}_{sub}$ and $\mathcal{S}_{sub}$.

Conversely, this means that $\mathcal{P}_{sub}$ and $\mathcal{S}_{sub}$ must have a problem with under-detection. In fact, this reflects our experience when carrying out multiple experiments (not shown) in which we tested alternative time windows to better detect seasonal subsurface scattering signals. Irrespective of the number of years and the choice of seasonal/monthly subsets, the method unfortunately failed by and large to pick up subsurface scattering signals in some climatic zones with a dry season such as over the Sahel or southern Africa. The main cause of the problem appears to be that in these environments, as can be seen in Fig. 3, θ_E typically varies little over the dry season while σ^0 may show relatively strong signal fluctuations. While this mismatch of signal magnitudes at the dry edge is not a problem when computing rank correlations, it impairs the capability to determine a best-fitting model $\mathcal{M}_0$ or $\mathcal{M}_1$. Therefore, we conclude that, given the properties of the σ^0 and θ_E time series, $\mathcal{P}_{sub}$ and $\mathcal{S}_{sub}$ are not as robust and sensitive as $\mathcal{P}_{ano}$, leading to a relatively strong under-estimation of subsurface scattering areas.

This conclusion is corroborated when using the three indicators for masking ASCAT soil moisture retrievals, and comparing the accuracy statistics of the ASCAT SSM data before and after masking. For this task we use the Pearson correlation R between the ASCAT SSM and the ERA5-Land soil moisture data calculated for each pixel over the complete time series. It is one of the most frequently used metrics in soil moisture validation studies [16] and has in our context the advantages that it can be computed everywhere and reveals rich spatial patterns in arid regions. This distinguishes it from other commonly used validation metrics that either show consistently low values in dry regions (e.g., the unbiased root mean square difference) or cannot be computed in subsurface scattering areas due to a violation of basic assumptions in the error models as in the case of triple collocation [15].

The global map of R without any masking of the subsurface scattering effects is shown in Fig. 8a. One can observe that desert regions are dominated by negative R values. However, there are also some desert areas where R is around zero or even slightly positive. An example is the Ar Rub' Al Khali desert in the southern part of the Arabian peninsula. It is the world's largest continuous sand desert covering an area of over 522,000 km^2, with huge dunes dominating much of the landscape [61]. In this case, the absence of subsurface scattering signals can be explained by deep layers of sand that "swallow" the radar pulses. On the other hand, subsurface scattering is strong in many of the stony and rocky desert regions of the Arabian peninsula.

<center>< Fig. 8 ></center>

The strong subsurface scattering signals in desert regions leave a strong imprint on the histogram of R shown in Fig. 9, with a significant portion of the ASCAT pixels (21.05 %) having R values smaller than zero. To mask these erroneous ASCAT retrievals one can apply different thresholds to the three global indicator maps shown in Fig. 5. The choice of the three thresholds is a trade-off between masking valid ASCAT pixels and missing erroneous ASCAT retrievals while taking the uncertainties of the three indicators themselves into account. Fig. 9 shows the resulting R histograms when applying static masks created with the same noise thresholds as used above (0.1 for $\mathcal{P}_{ano}$ and $\mathcal{P}_{sub}$, and 0.005 m^2 m^{-2} for $\mathcal{S}_{sub}$). One can see that $\mathcal{P}_{sub}$ and $\mathcal{S}_{sub}$ are both able to mask strong subsurface scattering signals (large negative R values) but largely fail to capture weaker ones (small negative R values). On the other hand, $\mathcal{P}_{ano}$ removes all pixels with negative R values. This, however, comes at the expense of masking also many regions where ASCAT retrievals are of good quality during the wet season, such as in the Sahel zone or in southern Africa. In these regions, a better solution is to mask ASCAT retrievals affected by subsurface scattering only during the dry season while retaining the retrievals from the wetter parts of the year. Therefore, we constructed monthly subsurface scattering masks by applying the threshold of 0.1 to monthly $\mathcal{P}_{ano}$ values and masking only pixels permanently when this threshold is exceeded for more than nine months. When recomputing R values after masking one finds that some negative R values persist, but this drawback is more than compensated for by the fact that both the number of pixels and their correlation increase significantly (compare the red to the green and blue lines in Fig. 5).

<center>< Fig. 9 ></center>

The recomputed R values are shown in Fig. 8b together with the permanently masked subsurface scattering areas. One can see that in combination with the other masks for dense vegetation, wetlands, and snow/frost the subsurface scattering mask ensures that only physically meaningful ASCAT SSM retrievals are retained. The figure is also useful to rate the relative importance of factors impacting the quality of ASCAT SSM retrievals. Normally, C-band sensors are held to be sub-optimal for soil moisture retrieval due to their limited capability to penetrate vegetation and soil [62]. However, the spatial extent of subsurface scattering areas is comparable to the extent of dense forest regions where soil moisture retrieval is not possible due to the high extinction of the C-band waves by the vegetation layer. Therefore, with the current generation of soil moisture retrieval algorithms, the transparency of dry upper soil layers is as much of a problem as the opaqueness of tropical forests and other dense vegetation regions. This may change with a new generation of soil moisture retrieval models that incorporate the exponential term $\psi e^{-\xi\theta}$ proposed by [33] or more elaborate formulations of subsurface scattering effects.

VII. CONCLUSIONS

This study has shown that subsurface scattering is the largest source of errors in the current version of the ASCAT soil moisture data as provided by EUMETSAT H SAF. The errors are most pronounced and widespread in desert regions, but they also extend widely into other climate zones with a dry season. In the past, due to the lack of a correct explanation, errors caused by subsurface scattering have been misinterpreted, for example, as topographic effects or changes in soil surface roughness and vegetation. With the knowledge gained in this study, the design of ASCAT soil moisture validation and application experiments can be improved, and conclusions drawn in previous ASCAT studies can be re-examined.

To quantify subsurface scattering effects, three indicators were used in this study. Two of them, the probability of detecting subsurface scattering, $\mathcal{P}_{sub}$, and the subsurface scattering signal strength, $\mathcal{S}_{sub}$, are based on a method that assesses the capability of two backscatter models (one with and one without a subsurface scattering term) to explain the observed behavior of ASCAT backscatter measurements with changing soil moisture conditions as captured by in situ and modeled soil moisture data sets. The merit of the method is that it is physically based, revealing pronounced spatial patterns, particularly in desert regions. However, it is not very robust against data outliers and differences in signal dynamics. As a result, $\mathcal{P}_{sub}$ and $\mathcal{S}_{sub}$ underestimate the extent of subsurface scattering areas while at the same time exhibiting spurious signals over higher latitude/altitude regions with seasonal snow cover and water bodies.

The third indicator is the probability of the occurrence of backscatter anomalies, $\mathcal{P}_{ano}$, which is a statistical method that looks for the "fingerprints" of subsurface scattering, i.e., an anti-correlation between backscatter and soil moisture. Even though there is a certain risk that it overestimates the extent of subsurface scattering, results obtained in this study suggest that, at the spatial scale of ASCAT, it is a robust indicator that exhibits the expected dependencies on external variables and classes well. Furthermore, it can be computed on a monthly basis, making it possible to use it for masking only measurements acquired during the dry season.

On a global scale, the three subsurface indicators exhibit the expected behavior, with subsurface scattering detected predominately in the arid climate zone, continental climates with dry summer, and the hot-summer Mediterranean climate. In these regions, the soil is typically bare or covered by low to medium vegetation, and soils tend to be poorly developed with a large fraction of coarse fragments in the soil profile. Nevertheless, there is great spatial variability on a local to regional scale that is not captured by ASCAT. This shows the need for further research to better understand environmental conditions and soil profile properties that give rise to subsurface scattering. Much can be learned from high-resolution Synthetic Aperture Radar (SAR) backscatter measurements that can be more readily related to in situ observations than is the case for ASCAT. For example, Ullmann et al. [63] analyzed Sentinel-1 SAR time series over the Atacama Desert, finding that thick atmospheric dust deposits on top of subsurface ce-

mented crusts give rise to strong subsurface scattering effects.

The results of this study are relevant not only for ASCAT but for any active microwave sensor operating at lower microwave frequencies. As the penetration depth increases with the wavelengths, a correct treatment of subsurface scattering effects might be even more challenging for sensors operating at S-, L-, and P-band. Furthermore, subsurface scattering is not only important in the context of soil moisture studies but for any effort to map land surface properties (vegetation, land cover, etc.) under dry climatic conditions. However, for the time being, there are no provisions for treating subsurface scattering effects in soil moisture and biomass retrievals from upcoming missions such as NISAR [64] or BIOMASS [65].

Within the context of the H SAF, the next step will be to investigate retrieval approaches that are able to deal with the ambiguity of the backscatter signal over subsurface scattering areas. Drawing from the experiences with ASCAT wind retrievals [66], a solution might be to provide two soil moisture values and then apply constraints to select the most likely solution. As long as no solution to the subsurface scattering problem exists, users of H SAF ASCAT soil moisture data can mask subsurface scattering effects using one of the indicators developed in this study and setting a threshold to match their requirements. As a baseline, we recommend using the monthly subsurface scattering masks developed within this study. Together with all indicators and ancillary data, it is available from the TU Wien Research Data repository (DOI: https://doi.org/10.48436/9a2y9-e5z14).

REFERENCES

[1] J. Figa-Saldaña, J. J. W. Wilson, E. P. W. Attema, R. Gelsthorpe, M. R. Drinkwater, and A. Stoffelen, "The advanced scatterometer (ASCAT) on the meteorological operational (MetOp) platform: A follow on for european wind scatterometers," *Canadian Journal of Remote Sensing*, vol. 28, no. 3, pp. 404–412, 2002.

[2] Z. Bartalis, W. Wagner, V. Naeimi, S. Hasenauer, K. Scipal, H. Bonekamp, J. Figa, and C. Anderson, "Initial soil moisture retrievals from the METOP-a advanced scatterometer (ASCAT)," *Geophysical Research Letters*, vol. 34, no. 20, p. L20401, 10 2007. [Online]. Available: http://doi.wiley.com/10.1029/2007GL031088

[3] D. B. Lindell and D. G. Long, "High-resolution soil moisture retrieval with ASCAT," *IEEE Geoscience and Remote Sensing Letters*, vol. 13, no. 7, pp. 972–976, 7 2016. [Online]. Available: http://ieeexplore.ieee.org/document/7466093/

[4] R. Quast, C. Albergel, J.-C. Calvet, and W. Wagner, "A generic first-order radiative transfer modelling approach for the inversion of soil and vegetation parameters from scatterometer observations," *Remote Sensing*, vol. 11, no. 3, p. 285, 2 2019. [Online]. Available: http://www.mdpi.com/2072-4292/11/3/285

[5] F. Aires, P. Weston, P. Rosnay, and D. Fairbairn, "Statistical approaches to assimilate ASCAT soil moisture information—i. methodologies and first assessment," *Quarterly Journal of the Royal Meteorological Society*, vol. 147, no. 736, pp. 1823–1852, 4 2021. [Online]. Available: https://onlinelibrary.wiley.com/doi/10.1002/qj.3997

[6] W. Wagner, S. Hahn, R. Kidd, T. Melzer, Z. Bartalis, S. Hasenauer, J. Figa-Saldaña, P. de Rosnay, A. Jann, S. Schneider, J. Komma, G. Kubu, K. Brugger, C. Aubrecht, J. Züger, U. Gangkofner, S. Kienberger, L. Brocca, Y. Wang, G. Blöschl, J. Eitzinger, and K. Steinnocher, "The ASCAT soil moisture product: A review of its specifications, validation results, and emerging applications," *Meteorologische Zeitschrift*, vol. 22, no. 1, pp. 5–33, 2 2013. [Online]. Available: http://www.schweizerbart.de/

[7] L. Brocca, W. T. Crow, L. Ciabatta, C. Massari, P. de Rosnay, M. Enenkel, S. Hahn, G. Amarnath, S. Camici, A. Tarpanelli, and W. Wagner, "A review of the applications of ASCAT soil moisture products," *IEEE Journal of Selected Topics in Applied Earth Observations and Remote Sensing*, vol. 10, no. 5, pp. 2285–2306, 5 2017. [Online]. Available: https://ieeexplore.ieee.org/document/7843617/

[8] R. A. M. De Jeu, W. Wagner, T. R. H. Holmes, A. J. Dolman, N. C. Van De Giesen, and J. Friesen, "Global soil moisture patterns observed by space borne microwave radiometers and scatterometers," *Surveys in Geophysics*, vol. 29, no. 4, pp. 399–420, 10 2008. [Online]. Available: http://link.springer.com/10.1007/s10712-008-9044-0

[9] A. Al Bitar, A. Mialon, Y. H. Kerr, F. Cabot, P. Richaume, E. Jacquette, A. Quesney, A. Mahmoodi, S. Tarot, M. Parrens, A. Al-Yaari, T. Pellarin, N. Rodriguez-Fernandez, and J.-P. Wigneron, "The global SMOS level 3 daily soil moisture and brightness temperature maps," *Earth System Science Data*, vol. 9, no. 1, pp. 293–315, 6 2017. [Online]. Available: https://essd.copernicus.org/articles/9/293/2017/

[10] S. K. Chan, R. Bindlish, P. E. O'Neill, E. Njoku, T. Jackson, A. Colliander, F. Chen, M. Burgin, S. Dunbar, J. Piepmeier, S. Yueh, D. Entekhabi, M. H. Cosh, T. Caldwell, J. Walker, X. Wu, A. Berg, T. Rowlandson, A. Pacheco, H. McNairn, M. Thibeault, J. Martinez-Fernandez, A. Gonzalez-Zamora, M. Seyfried, D. Bosch, P. Starks, D. Goodrich, J. Prueger, M. Palecki, E. E. Small, M. Zreda, J.-C. Calvet, W. T. Crow, and Y. Kerr, "Assessment of the SMAP passive soil moisture product," *IEEE Transactions on Geoscience and Remote Sensing*, vol. 54, no. 8, pp. 4994–5007, 8 2016. [Online]. Available: http://ieeexplore.ieee.org/document/7478653/

[11] P. Yao, H. Lu, J. Shi, T. Zhao, K. Yang, M. H. Cosh, D. J. S. Gianotti, and D. Entekhabi, "A long term global daily soil moisture dataset derived from AMSR-e and AMSR2 (2002–2019)," *Scientific Data*, vol. 8, no. 1, p. 143, 12 2021. [Online]. Available: http://www.nature.com/articles/s41597-021-00925-8

[12] A. Gruber, T. Scanlon, R. van der Schalie, W. Wagner, and W. Dorigo, "Evolution of the ESA CCI soil moisture climate data records and their underlying merging methodology," *Earth System Science Data*, vol. 11, no. 2, pp. 717–739, 5 2019. [Online]. Available: https://essd.copernicus.org/articles/11/717/2019/

[13] J. Yin, X. Zhan, and J. Liu, "NOAA satellite soil moisture operational product system (SMOPS) version 3.0 generates higher accuracy blended satellite soil moisture," *Remote Sensing*, vol. 12, no. 17, p. 2861, 9 2020. [Online]. Available: https://www.mdpi.com/2072-4292/12/17/2861

[14] A. Gruber, W. A. Dorigo, W. Crow, and W. Wagner, "Triple collocation-based merging of satellite soil moisture retrievals," *IEEE Transactions on Geoscience and Remote Sensing*, vol. 55, no. 12, pp. 6780–6792, 12 2017. [Online]. Available: http://ieeexplore.ieee.org/document/8046118/

[15] A. Gruber, G. De Lannoy, C. Albergel, A. Al-Yaari, L. Brocca, J.-C. Calvet, A. Colliander, M. Cosh, W. Crow, W. Dorigo, C. Draper, M. Hirschi, Y. Kerr, A. Konings, W. Lahoz, K. McColl, C. Montzka, J. Muñoz-Sabater, J. Peng, R. Reichle, P. Richaume, C. Rüdiger, T. Scanlon, R. van der Schalie, J.-P. Wigneron, and W. Wagner, "Validation practices for satellite soil moisture retrievals: What are (the) errors?" *Remote Sensing of Environment*, vol. 244, p. 111806, 7 2020. [Online]. Available: https://linkinghub.elsevier.com/retrieve/pii/S0034425720301760

[16] C. Montzka, M. Cosh, B. Bayat, A. Al Bitar, A. Berg, R. Bindlish, H. Bogena, J. Bolten, F. Cabot, T. Caldwell, S. Chan, A. Colliander, W. Crow, N. Das, G. De Lannoy, W. Dorigo, S. Evett, A. Gruber, S. Hahn, S. Jagdhuber, S. Jones, Y. Kerr, S. Kim, C. Koyama, M. Kurum, E. Lopez-Baeza, F. Mattia, K. McColl, S. Mecklenburg, P. Mohanty, P. O'Neill, D. Or, T. Pellarin, G. Petropoulos, M. Piles, R. Reichle, N. Rodriguez-Fernandez, C. Rüdiger, T. Scanlon, R. Schwartz, D. Spengler, P. Srivastava, S. Suman, R. van der Schalie, W. Wagner, U. Wegmuller, J.-P. Wigneron, F. Camacho, and J. Nickeson, "Soil moisture product validation good practices protocol," *CEOS Land Product Validation Protocols*, pp. 1–123, 2020, publisher: Land Product Validation Subgroup, Working Group on Calibration and Validation, Committee on Earth Observation Satellites (CEOS). [Online]. Available: http://lpvs.gsfc.nasa.gov/documents.html

[17] L. Brocca, S. Hasenauer, T. Lacava, F. Melone, T. Moramarco, W. Wagner, W. Dorigo, P. Matgen, J. Martínez-Fernández, P. Llorens, J. Latron, C. Martin, and M. Bittelli, "Soil moisture estimation through ASCAT and AMSR-e sensors: An intercomparison and validation study across europe," *Remote Sensing of Environment*, vol. 115, no. 12, pp. 3390–3408, 12 2011. [Online]. Available: https://linkinghub.elsevier.com/retrieve/pii/S0034425711002756

[18] A. Al-Yaari, J.-P. Wigneron, A. Ducharne, Y. Kerr, W. Wagner, G. De Lannoy, R. Reichle, A. Al Bitar, W. Dorigo, P. Richaume, and A. Mialon, "Global-scale comparison of passive (SMOS) and active (ASCAT) satellite based microwave soil moisture retrievals with soil moisture simulations (MERRA-land)," *Remote Sensing of Environment*, vol. 152, pp. 614–626, 9 2014. [Online]. Available: https://linkinghub.elsevier.com/retrieve/pii/S0034425714002612

[19] F. Chen, W. T. Crow, R. Bindlish, A. Colliander, M. S. Burgin, J. Asanuma, and K. Aida, "Global-scale evaluation of SMAP, SMOS and ASCAT soil moisture products using triple collocation," *Remote Sensing of Environment*, vol. 214, pp. 1–13, 9 2018. [Online]. Available: https://linkinghub.elsevier.com/retrieve/pii/S0034425718302293

[20] H. Kim, J.-P. Wigneron, S. Kumar, J. Dong, W. Wagner, M. H. Cosh, D. D. Bosch, C. H. Collins, P. J. Starks, M. Seyfried, and V. Lakshmi, "Global scale error assessments of soil moisture estimates from microwave-based active and passive satellites and land surface models over forest and mixed irrigated/dryland agriculture regions," *Remote Sensing of Environment*, vol. 251, p. 112052, 12 2020. [Online]. Available: https://linkinghub.elsevier.com/retrieve/pii/S0034425720304223

[21] H. E. Beck, M. Pan, D. G. Miralles, R. H. Reichle, W. A. Dorigo, S. Hahn, J. Sheffield, L. Karthikeyan, G. Balsamo, R. M. Parinussa, A. I. J. M. van Dijk, J. Du, J. S. Kimball, N. Vergopolan, and E. F. Wood, "Evaluation of 18 satellite- and model-based soil moisture products using in situ measurements from 826 sensors," *Hydrology and Earth System Sciences*, vol. 25, no. 1, pp. 17–40, 1 2021. [Online]. Available: https://hess.copernicus.org/articles/25/17/2021/

[22] W. Dorigo, I. Himmelbauer, D. Aberer, L. Schremmer, I. Petrakovic, L. Zappa, W. Preimesberger, A. Xaver, F. Annor, J. Ardö, D. Baldocchi, M. Bitelli, G. Blöschl, H. Bogena, L. Brocca, J.-C. Calvet, J. J. Camarero, G. Capello, M. Choi, M. C. Cosh, N. van de Giesen, I. Hajdu, I. Ikonen, K. H. Jensen, K. D. Kanniah, I. de Kat, G. Kirchengast, P. Kumar Rai, J. Kyrouac, K. Larson, S. Liu, A. Loew, M. Moghaddam, J. Martínez Fernández, C. Mattar Bader, R. Morbidelli, J. P. Musial, E. Osenga, M. A. Palecki, T. Pellarin, G. P. Petropoulos, I. Pfeil, J. Powers, A. Robock, C. Rüdiger, U. Rummel, M. Strobel, Z. Su, R. Sullivan, T. Tagesson, A. Varlagin, M. Vreugdenhil, J. Walker, J. Wen, F. Wenger, J. P. Wigneron, M. Woods, K. Yang, Y. Zeng, X. Zhang, M. Zreda, S. Dietrich, A. Gruber, P. van Oevelen, W. Wagner, K. Scipal, M. Drusch, and R. Sabia, "The international soil moisture network: serving earth system science for over a decade," *Hydrology and Earth System Sciences*, vol. 25, no. 11, pp. 5749–5804, 11 2021. [Online]. Available: https://hess.copernicus.org/articles/25/5749/2021/

[23] H. Hersbach, B. Bell, P. Berrisford, S. Hirahara, A. Horányi, J. Muñoz-Sabater, J. Nicolas, C. Peubey, R. Radu, D. Schepers, A. Simmons, C. Soci, S. Abdalla, X. Abellan, G. Balsamo, P. Bechtold, G. Biavati, J. Bidlot, M. Bonavita, G. Chiara, P. Dahlgren, D. Dee, M. Diamantakis, R. Dragani, J. Flemming, R. Forbes, M. Fuentes, A. Geer, L. Haimberger, S. Healy, R. J. Hogan, E. Hólm, M. Janisková, S. Keeley, P. Laloyaux, P. Lopez, C. Lupu, G. Radnoti, P. Rosnay, I. Rozum, F. Vamborg, S. Villaume, and J. Thépaut, "The ERA5 global reanalysis," *Quarterly Journal of the Royal Meteorological Society*, vol. 146, no. 730, pp. 1999–2049, 7 2020. [Online]. Available: https://onlinelibrary.wiley.com/doi/10.1002/qj.3803

[24] M. Rodell, P. R. Houser, U. Jambor, J. Gottschalck, K. Mitchell, C.-J. Meng, K. Arsenault, B. Cosgrove, J. Radakovich, M. Bosilovich, J. K. Entin, J. P. Walker, D. Lohmann, and D. Toll, "The global land data assimilation system," *Bulletin of the American Meteorological Society*, vol. 85, no. 3, pp. 381–394, 3 2004. [Online]. Available: https://journals.ametsoc.org/doi/10.1175/BAMS-85-3-381

[25] D. Entekhabi, R. H. Reichle, R. D. Koster, and W. T. Crow, "Performance metrics for soil moisture retrievals and application requirements," *Journal of Hydrometeorology*, vol. 11, no. 3, pp. 832–840, 6 2010. [Online]. Available: http://journals.ametsoc.org/doi/10.1175/2010JHM1223.1

[26] L. Brocca, F. Melone, T. Moramarco, W. Wagner, and S. Hasenauer, "ASCAT soil wetness index validation through in situ and modeled soil moisture data in central italy," *Remote Sensing of Environment*, vol. 114, no. 11, pp. 2745–2755, 11 2010. [Online]. Available: https://linkinghub.elsevier.com/retrieve/pii/S0034425710001999

[27] K. Scipal, T. Holmes, R. de Jeu, V. Naeimi, and W. Wagner, "A possible solution for the problem of estimating the error structure of global soil moisture data sets," *Geophysical Research Letters*, vol. 35, no. 24, p. L24403, 12 2008. [Online]. Available: http://doi.wiley.com/10.1029/2008GL035599

[28] C.-H. Su, D. Ryu, W. T. Crow, and A. W. Western, "Beyond triple collocation: Applications to soil moisture monitoring: Beyond triple collocation," *Journal of Geophysical Research: Atmospheres*, vol. 119, no. 11, pp. 6419–6439, 6 2014. [Online]. Available: http://doi.wiley.com/10.1002/2013JD021043

[29] ——, "Stand-alone error characterisation of microwave satellite soil moisture using a fourier method," *Remote Sensing of Environment*, vol. 154, pp. 115–126, 11 2014. [Online]. Available: https://linkinghub.elsevier.com/retrieve/pii/S0034425714003113

[30] M. Parrens, E. Zakharova, S. Lafont, J.-C. Calvet, Y. Kerr, W. Wagner, and J.-P. Wigneron, "Comparing soil moisture retrievals from SMOS and ASCAT over france," *Hydrology and Earth System Sciences*, vol. 16, no. 2, pp. 423–440, 2 2012. [Online]. Available: https://hess.copernicus.org/articles/16/423/2012/

[31] W. A. Dorigo, K. Scipal, R. M. Parinussa, Y. Y. Liu, W. Wagner, R. A. M. De Jeu, and V. Naeimi, "Error characterisation of global active and passive microwave soil moisture datasets," *Hydrology and Earth System Sciences*, vol. 14, no. 12, pp. 2605–2616, 12 2010. [Online]. Available: https://hess.copernicus.org/articles/14/2605/2010/

[32] K. Morrison and W. Wagner, "Explaining anomalies in SAR and scatterometer soil moisture retrievals from dry soils with subsurface scattering," *IEEE Transactions on Geoscience and Remote Sensing*, vol. 58, no. 3, pp. 2190–2197, 3 2020. [Online]. Available: https://ieeexplore.ieee.org/document/8936549/

[33] W. Wagner, R. Lindorfer, T. Melzer, S. Hahn, B. Bauer-Marschallinger, K. Morrison, J.-C. Calvet, S. Hobbs, R. Quast, I. Greimeister-Pfeil, and M. Vreugdenhil, "Widespread occurrence of anomalous c-band backscatter signals in arid environments caused by subsurface scattering," *Remote Sensing of Environment*, vol. 276, p. 113025, 7 2022. [Online]. Available: https://linkinghub.elsevier.com/retrieve/pii/S0034425722001390

[34] W. Dorigo, W. Wagner, C. Albergel, F. Albrecht, G. Balsamo, L. Brocca, D. Chung, M. Ertl, M. Forkel, A. Gruber, E. Haas, P. D. Hamer, M. Hirschi, J. Ikonen, R. de Jeu, R. Kidd, W. Lahoz, Y. Y. Liu, D. Miralles, T. Mistelbauer, N. Nicolai-Shaw, R. Parinussa, C. Pratola, C. Reimer, R. van der Schalie, S. I. Seneviratne, T. Smolander, and P. Lecomte, "ESA CCI soil moisture for improved earth system understanding: State-of-the art and future directions," *Remote Sensing of Environment*, vol. 203, pp. 185–215, 12 2017. [Online]. Available: https://linkinghub.elsevier.com/retrieve/pii/S0034425717303061

[35] C. Paulik, W. Dorigo, W. Wagner, and R. Kidd, "Validation of the ASCAT Soil Water Index using in situ data from the International Soil Moisture Network," *International Journal of Applied Earth Observation and Geoinformation*, vol. 30, pp. 1–8, Aug. 2014. [Online]. Available: https://linkinghub.elsevier.com/retrieve/pii/S0303243414000099

[36] B. Bauer-Marschallinger, C. Paulik, S. Hochstöger, T. Mistelbauer, S. Modanesi, L. Ciabatta, C. Massari, L. Brocca, and W. Wagner, "Soil Moisture from Fusion of Scatterometer and SAR: Closing the Scale Gap with Temporal Filtering," *Remote Sensing*, vol. 10, no. 7, p. 1030, Jun. 2018. [Online]. Available: http://www.mdpi.com/2072-4292/10/7/1030

[37] H. Kim, W. T. Crow, W. Wagner, X. Li, and V. Lakshmi, "A bayesian machine learning method to explain the error characteristics of global-scale soil moisture products," *Remote Sensing of Environment*, vol. 296, p. 113718, 2023. [Online]. Available: https://linkinghub.elsevier.com/retrieve/pii/S0034425723002699

[38] W. Wagner, J. Noll, M. Borgeaud, and H. Rott, "Monitoring soil moisture over the canadian prairies with the ERS scatterometer," *IEEE Transactions on Geoscience and Remote Sensing*, vol. 37, no. 1, pp. 206–216, 1 1999. [Online]. Available: http://ieeexplore.ieee.org/document/739155/

[39] V. Naeimi, K. Scipal, Z. Bartalis, S. Hasenauer, and W. Wagner, "An improved soil moisture retrieval algorithm for ERS and METOP scatterometer observations," *IEEE Transactions on Geoscience and Remote Sensing*, vol. 47, no. 7, pp. 1999–2013, 7 2009. [Online]. Available: http://ieeexplore.ieee.org/document/4814564/

[40] S. Hahn, W. Wagner, S. C. Steele-Dunne, M. Vreugdenhil, and T. Melzer, "Improving ASCAT soil moisture retrievals with an enhanced spatially variable vegetation parameterization," *IEEE Transactions on Geoscience and Remote Sensing*, vol. 59, no. 10, pp. 8241–8256, 10 2021. [Online]. Available: https://ieeexplore.ieee.org/document/9300194/

[41] W. Wagner, G. Lemoine, M. Borgeaud, and H. Rott, "A study of vegetation cover effects on ERS scatterometer data," *IEEE Transactions on Geoscience and Remote Sensing*, vol. 37, no. 2, pp. 938–948, 3 1999. [Online]. Available: http://ieeexplore.ieee.org/document/752212/

[42] I. Pfeil, M. Vreugdenhil, S. Hahn, W. Wagner, P. Strauss, and G. Blöschl, "Improving the seasonal representation of ASCAT soil moisture and vegetation dynamics in a temperate climate," *Remote Sensing*, vol. 10, no. 11, p. 1788, 11 2018. [Online]. Available: http://www.mdpi.com/2072-4292/10/11/1788

[43] E. P. W. Attema and F. T. Ulaby, "Vegetation modeled as a water cloud," *Radio Science*, vol. 13, no. 2, pp. 357–364, 3 1978. [Online]. Available: http://doi.wiley.com/10.1029/RS013i002p00357

[44] A. Dostálová, M. Doubková, D. Sabel, B. Bauer-Marschallinger, and W. Wagner, "Seven years of advanced synthetic aperture radar (ASAR) global monitoring (GM) of surface soil moisture over africa," *Remote Sensing*, vol. 6, no. 8, pp. 7683–7707, 8 2014. [Online]. Available: http://www.mdpi.com/2072-4292/6/8/7683

[45] K. A. McColl, D. Entekhabi, and M. Piles, "Uncertainty analysis of soil moisture and vegetation indices using aquarius scatterometer observations," *IEEE Transactions on Geoscience and Remote Sensing*, vol. 52, no. 7, pp. 4259–4272, 7 2014. [Online]. Available: http://ieeexplore.ieee.org/document/6619434/

[46] T. Ullmann, K. Serfas, C. Büdel, M. Padashi, and R. Baumhauer, "Data processing, feature extraction, and time-series analysis of sentinel-1 synthetic aperture radar (SAR) imagery: Examples from damghan and bajestan playa (iran)," *Zeitschrift für Geomorphologie, Supplementary Issues*, vol. 62, no. 1, pp. 9–39, 6 2019, place: Stuttgart, Germany Publisher: Schweizerbart Science Publishers. [Online]. Available: http://dx.doi.org/10.1127/zfg_suppl/2019/0524

[47] M. J. Escorihuela and P. Quintana-Seguí, "Comparison of remote sensing and simulated soil moisture datasets in mediterranean landscapes," *Remote Sensing of Environment*, vol. 180, pp. 99–114, 7 2016. [Online]. Available: https://linkinghub.elsevier.com/retrieve/pii/S0034425716300748

[48] M. Zribi, M. Foucras, N. Baghdadi, J. Demarty, and S. Muddu, "A new reflectivity index for the retrieval of surface soil moisture from radar data," *IEEE Journal of Selected Topics in Applied Earth Observations and Remote Sensing*, vol. 14, pp. 818–826, 2021. [Online]. Available: https://ieeexplore.ieee.org/document/9237103/

[49] A. Fung and K. Chen, "An update on the IEM surface backscattering model," *IEEE Geoscience and Remote Sensing Letters*, vol. 1, no. 2, pp. 75–77, 4 2004. [Online]. Available: http://ieeexplore.ieee.org/document/1291385/

[50] P. Dubois, J. van Zyl, and T. Engman, "Measuring soil moisture with imaging radars," *IEEE Transactions on Geoscience and Remote Sensing*, vol. 33, no. 4, pp. 915–926, 7 1995. [Online]. Available: http://ieeexplore.ieee.org/document/406677/

[51] S. Hahn, C. Reimer, M. Vreugdenhil, T. Melzer, and W. Wagner, "Dynamic characterization of the incidence angle dependence of backscatter using metop ASCAT," *IEEE Journal of Selected Topics in Applied Earth Observations and Remote Sensing*, vol. 10, no. 5, pp. 2348–2359, 5 2017. [Online]. Available: https://ieeexplore.ieee.org/document/7815274/

[52] H SAF, "Product User Manual, Metop ASCAT Surface Soil Moisture Climate Data Record v7 12.5 km sampling (H119) and Extension (H120), v1.2, 2022." 2022. [Online]. Available: https://hsaf.meteoam.it/Products/Detail?prod=H119

[53] B. Lehner and P. Döll, "Development and validation of a global database of lakes, reservoirs and wetlands," *Journal of Hydrology*, vol. 296, no. 1, pp. 1–22, 8 2004. [Online]. Available: https://linkinghub.elsevier.com/retrieve/pii/S0022169404001404

[54] J. Muñoz-Sabater, E. Dutra, A. Agustí-Panareda, C. Albergel, G. Arduini, G. Balsamo, S. Boussetta, M. Choulga, S. Harrigan, H. Hersbach, B. Martens, D. G. Miralles, M. Piles, N. J. Rodríguez-Fernández, E. Zsoter, C. Buontempo, and J.-N. Thépaut, "ERA5-land: a state-of-the-art global reanalysis dataset for land applications," *Earth System Science Data*, vol. 13, no. 9, pp. 4349–4383, 9 2021. [Online]. Available: https://essd.copernicus.org/articles/13/4349/2021/

[55] W. Dorigo, A. Xaver, M. Vreugdenhil, A. Gruber, A. Hegyiová, A. Sanchis-Dufau, D. Zamojski, C. Cordes, W. Wagner, and M. Drusch, "Global Automated Quality Control of In Situ Soil Moisture Data from the International Soil Moisture Network," *Vadose Zone Journal*, vol. 12, no. 3, p. vzj2012.0097, Aug. 2013. [Online]. Available: http://doi.wiley.com/10.2136/vzj2012.0097

[56] R. Magagi and Y. Kerr, "Characterization of surface parameters over arid and semi-arid areas by use of ERS-1 windscatterometer," *Remote Sens-*

ing Reviews, vol. 15, no. 1, pp. 133–155, 2 1997. [Online]. Available: http://www.tandfonline.com/doi/abs/10.1080/02757259709532335

[57] L. Jarlan, E. Mougin, P. Frison, P. Mazzega, and P. Hiernaux, "Analysis of ERS wind scatterometer time series over sahel (mali)," *Remote Sensing of Environment*, vol. 81, no. 2, pp. 404–415, 8 2002. [Online]. Available: https://linkinghub.elsevier.com/retrieve/pii/S0034425702000159

[58] S. Louvet, T. Pellarin, A. al Bitar, B. Cappelaere, S. Galle, M. Grippa, C. Gruhier, Y. Kerr, T. Lebel, A. Mialon, E. Mougin, G. Quantin, P. Richaume, and P. de Rosnay, "SMOS soil moisture product evaluation over west-africa from local to regional scale," *Remote Sensing of Environment*, vol. 156, pp. 383–394, 1 2015. [Online]. Available: https://linkinghub.elsevier.com/retrieve/pii/S0034425714004015

[59] C. Fatras, F. Frappart, E. Mougin, P.-L. Frison, G. Faye, P. Borderies, and L. Jarlan, "Spaceborne altimetry and scatterometry backscattering signatures at c- and ku-bands over west africa," *Remote Sensing of Environment*, vol. 159, pp. 117–133, 3 2015. [Online]. Available: https://linkinghub.elsevier.com/retrieve/pii/S0034425714004891

[60] S. E. Nicholson, "The ITCZ and the seasonal cycle over equatorial africa," *Bulletin of the American Meteorological Society*, vol. 99, no. 2, pp. 337–348, 2 2018. [Online]. Available: https://journals.ametsoc.org/doi/10.1175/BAMS-D-16-0287.1

[61] H. S. Edgell, *Arabian Deserts*. Springer Netherlands, 2006. [Online]. Available: http://link.springer.com/10.1007/1-4020-3970-0

[62] D. Entekhabi, E. G. Njoku, P. E. O'Neill, K. H. Kellogg, W. T. Crow, W. N. Edelstein, J. K. Entin, S. D. Goodman, T. J. Jackson, J. Johnson, J. Kimball, J. R. Piepmeier, R. D. Koster, N. Martin, K. C. McDonald, M. Moghaddam, S. Moran, R. Reichle, J. C. Shi, M. W. Spencer, S. W. Thurman, L. Tsang, and J. Van Zyl, "The soil moisture active passive (SMAP) mission," *Proceedings of the IEEE*, vol. 98, no. 5, pp. 704–716, 5 2010. [Online]. Available: http://ieeexplore.ieee.org/document/5460980/

[63] T. Ullmann, T. Jagdhuber, D. Hoffmeister, S. M. May, R. Baumhauer, and O. Bubenzer, "Exploring sentinel-1 backscatter time series over the atacama desert (chile) for seasonal dynamics of surface soil moisture," *Remote Sensing of Environment*, vol. 285, p. 113413, 2 2023. [Online]. Available: https://linkinghub.elsevier.com/retrieve/pii/S0034425722005193

[64] P. Lal, G. Singh, N. N. Das, D. Entekhabi, R. Lohman, A. Colliander, D. K. Pandey, and R. Setia, "A multi-scale algorithm for the NISAR mission high-resolution soil moisture product," *Remote Sensing of Environment*, vol. 295, p. 113667, Sep. 2023. [Online]. Available: https://linkinghub.elsevier.com/retrieve/pii/S0034425723002183

[65] S. Quegan, T. Le Toan, J. Chave, J. Dall, J.-F. Exbrayat, D. H. T. Minh, M. Lomas, M. M. D'Alessandro, P. Paillou, K. Papathanassiou, F. Rocca, S. Saatchi, K. Scipal, H. Shugart, T. L. Smallman, M. J. Soja, S. Tebaldini, L. Ulander, L. Villard, and M. Williams, "The European Space Agency BIOMASS mission: Measuring forest above-ground biomass from space," *Remote Sensing of Environment*, vol. 227, pp. 44–60, Jun. 2019. [Online]. Available: https://linkinghub.elsevier.com/retrieve/pii/S0034425719301233

[66] W. Lin, M. Portabella, A. Stoffelen, and A. Verhoef, "On the characteristics of ASCAT wind direction ambiguities," *Atmospheric Measurement Techniques*, vol. 6, no. 4, pp. 1053–1060, 4 2013. [Online]. Available: https://amt.copernicus.org/articles/6/1053/2013/

[67] H. E. Beck, N. E. Zimmermann, T. R. McVicar, N. Vergopolan, A. Berg, and E. F. Wood, "Present and future köppen-geiger climate classification maps at 1-km resolution," *Scientific Data*, vol. 5, no. 1, p. 180214, Oct 2018. [Online]. Available: https://doi.org/10.1038/sdata.2018.214

[68] Copernicus Climate Change Service. (2019) Land cover classification gridded maps from 1992 to present derived from satellite observation. copernicus climate change service (c3s) climate data store (cds). [Online]. Available: https://doi.org/10.24381/cds.006f2c9a

[69] L. Poggio, L. M. de Sousa, N. H. Batjes, G. B. M. Heuvelink, B. Kempen, E. Ribeiro, and D. Rossiter, "SoilGrids 2.0: producing soil information for the globe with quantified spatial uncertainty," *SOIL*, vol. 7, no. 1, pp. 217–240, 6 2021. [Online]. Available: https://soil.copernicus.org/articles/7/217/2021/

[70] European Space Agency, Copernicus Contributing Missions Online. (2022) Copernicus dem - global and european digital elevation model (cop-dem). [Online]. Available: https://doi.org/10.5270/ESA-c5d3d65

[71] L. Hawker, P. Uhe, L. Paulo, J. Sosa, J. Savage, C. Sampson, and J. Neal, "A 30 m global map of elevation with forests and buildings removed," *Environmental Research Letters*, vol. 17, no. 2, p. 024016, feb 2022. [Online]. Available: https://dx.doi.org/10.1088/1748-9326/ac4d4f

[72] NOAA National Centers for Environmental Information. (2022) Etopo 2022 15 arc-second global relief model. [Online]. Available: https://doi.org/10.25921/fd45-gt74

[73] Copernicus Global Land Service. (2018) Leaf area index and fraction absorbed of photosynthetically active radiation 10-daily gridded data from 1981 to present. [Online]. Available: https://doi.org/10.24381/cds.7e59b01a

[74] E. Mougin, P. Hiernaux, L. Kergoat, M. Grippa, P. de Rosnay, F. Timouk, V. Le Dantec, V. Demarez, F. Lavenu, M. Arjounin, T. Lebel, N. Soumaguel, E. Ceschia, B. Mougenot, F. Baup, F. Frappart, P. Frison, J. Gardelle, C. Gruhier, L. Jarlan, S. Mangiarotti, B. Sanou, Y. Tracol, F. Guichard, V. Trichon, L. Diarra, A. Soumaré, M. Koité, F. Dembélé, C. Lloyd, N. Hanan, C. Damesin, C. Delon, D. Serça, C. Galy-Lacaux, J. Seghieri, S. Becerra, H. Dia, F. Gangneron, and P. Mazzega, "The amma-catch gourma observatory site in mali: Relating climatic variations to changes in vegetation, surface hydrology, fluxes and natural resources," *Journal of Hydrology*, vol. 375, no. 1, pp. 14–33, 2009, surface processes and water cycle in West Africa, studied from the AMMA-CATCH observing system. [Online]. Available: https://www.sciencedirect.com/science/article/pii/S0022169409003825

[75] T. Tagesson, R. Fensholt, I. Guiro, M. O. Rasmussen, S. Huber, C. Mbow, M. Garcia, S. Horion, I. Sandholt, B. Holm-Rasmussen, F. M. Göttsche, M.-E. Ridler, N. Olén, J. Lundegard Olsen, A. Ehammer, M. Madsen, F. S. Olesen, and J. Ardö, "Ecosystem properties of semiarid savanna grassland in west africa and its relationship with environmental variability," *Global Change Biology*, vol. 21, no. 1, pp. 250–264, 2015. [Online]. Available: https://onlinelibrary.wiley.com/doi/abs/10.1111/gcb.12734

[76] J. Ardö, "A 10-year dataset of basic meteorology and soil properties in central sudan," *Dataset Papers in Geosciences*, vol. 2013, Nov 2012. [Online]. Available: https://doi.org/10.7167/2013/297973

[77] N. van de Giesen, R. Hut, and J. Selker, "The trans-african hydro-meteorological observatory (tahmo)," *WIREs Water*, vol. 1, no. 4, pp. 341–348, 2014. [Online]. Available: https://wires.onlinelibrary.wiley.com/doi/abs/10.1002/wat2.1034

[78] A. B. Smith, J. P. Walker, A. W. Western, R. I. Young, K. M. Ellett, R. C. Pipunic, R. B. Grayson, L. Siriwardena, F. H. S. Chiew, and H. Richter, "The murrumbidgee soil moisture monitoring network data set," *Water Resources Research*, vol. 48, no. 7, 2012. [Online]. Available: https://agupubs.onlinelibrary.wiley.com/doi/abs/10.1029/2012WR011976

[79] A. Al-Yaari, S. Dayau, C. Chipeaux, C. Aluome, A. Kruszewski, D. Loustau, and J.-P. Wigneron, "The aqui soil moisture network for satellite microwave remote sensing validation in south-western france," *Remote Sensing*, vol. 10, no. 11, 2018. [Online]. Available: https://www.mdpi.com/2072-4292/10/11/1839

[80] G. Blöschl, A. P. Blaschke, M. Broer, C. Bucher, G. Carr, X. Chen, A. Eder, M. Exner-Kittridge, A. Farnleitner, A. Flores-Orozco, P. Haas, P. Hogan, A. Kazemi Amiri, M. Oismüller, J. Parajka, R. Silasari, P. Stadler, P. Strauss, M. Vreugdenhil, W. Wagner, and M. Zessner, "The hydrological open air laboratory (hoal) in petzenkirchen: a hypothesis-driven observatory," *Hydrology and Earth System Sciences*, vol. 20, no. 1, pp. 227–255, 2016. [Online]. Available: https://hess.copernicus.org/articles/20/227/2016/

[81] K. H. Jensen and J. C. Refsgaard, "Hobe: The danish hydrological observatory," *Vadose Zone Journal*, vol. 17, no. 1, p. 180059, 2018. [Online]. Available: https://acsess.onlinelibrary.wiley.com/doi/abs/10.2136/vzj2018.03.0059

[82] A. Flammini, R. Morbidelli, C. Saltalippi, T. Picciafuoco, C. Corradini, and R. S. Govindaraju, "Reassessment of a semi-analytical field-scale infiltration model through experiments under natural rainfall events," *Journal of Hydrology*, vol. 565, pp. 835–845, 2018. [Online]. Available: https://www.sciencedirect.com/science/article/pii/S0022169418306723

[83] J. G. Alday, J. J. Camarero, J. Revilla, and V. Resco de Dios, "Similar diurnal, seasonal and annual rhythms in radial root expansion across two coexisting Mediterranean oak species," *Tree Physiology*, vol. 40, no. 7, pp. 956–968, 04 2020. [Online]. Available: https://doi.org/10.1093/treephys/tpaa041

[84] M. Riffard, F. Birgand, C. Loumagne, V. Andréassian, C. Kao, C. Chaumont, and P. Ansart, "ORACLE : an experimental site since 1962 for the study of hydrological hazards and biogeochemical processes," p. 2, 2006. [Online]. Available: https://hal.inrae.fr/hal-02588192

[85] A. González-Zamora, N. Sánchez, M. Pablos, and J. Martínez-Fernández, "Cci soil moisture assessment with smos soil moisture and in situ data under different environmental conditions and spatial scales in spain," *Remote Sensing of Environment*, vol. 225, pp. 469–482, 2019. [Online]. Available: https://www.sciencedirect.com/science/article/pii/S0034425718300166

[86] I. Ontel, A. Irimescu, G. Boldeanu, D. Mihailescu, C.-V. Angearu, A. Nertan, V. Craciunescu, and S. Negreanu, "Assessment of soil moisture anomaly sensitivity to detect drought spatio-temporal variability in romania," *Sensors*, vol. 21, no. 24, 2021. [Online]. Available: https://www.mdpi.com/1424-8220/21/24/8371

[87] J.-C. Calvet, N. Fritz, F. Froissard, D. Suquia, A. Petitpa, and B. Piguet, "In situ soil moisture observations for the cal/val of smos: the smosmania network," in *2007 IEEE International Geoscience and Remote Sensing Symposium*, 2007, pp. 1196–1199.

[88] H. Bogena, C. Montzka, J. Huisman, A. Graf, M. Schmidt, M. Stockinger, C. von Hebel, H. Hendricks-Franssen, J. van der Kruk, W. Tappe, A. Lücke, R. Baatz, R. Bol, J. Groh, T. Pütz, J. Jakobi, R. Kunkel, J. Sorg, and H. Vereecken, "The tereno-rur hydrological observatory: A multiscale multi-compartment research platform for the advancement of hydrological science," *Vadose Zone Journal*, vol. 17, no. 1, p. 180055, 2018. [Online]. Available: https://acsess.onlinelibrary.wiley.com/doi/abs/10.2136/vzj2018.03.0055

[89] F. Schlenz, J. T. dall'Amico, A. Loew, and W. Mauser, "Uncertainty assessment of the smos validation in the upper danube catchment," *IEEE Transactions on Geoscience and Remote Sensing*, vol. 50, no. 5, pp. 1517–1529, 2012.

[90] D. R. Cook, "Soil temperature and moisture profile (stamp) system handbook," 11 2016. [Online]. Available: https://www.osti.gov/biblio/1332724

[91] D. Baldocchi, E. Falge, L. Gu, R. Olson, D. Hollinger, S. Running, P. Anthoni, C. Bernhofer, K. Davis, R. Evans, J. Fuentes, A. Goldstein, G. Katul, B. Law, X. Lee, Y. Malhi, T. Meyers, J. Munger, W. Oechel, and F. Richardson, "Fluxnet: A new tool to study the temporal and spatial variability of ecosystem–scale carbon dioxide, water vapor, and energy flux densities," ©*2001 American Meteorological Society*, vol. 82, 11 2001.

[92] K. M. Larson, E. E. Small, E. D. Gutmann, A. L. Bilich, J. J. Braun, and V. U. Zavorotny, "Use of gps receivers as a soil moisture network for water cycle studies," *Geophysical Research Letters*, vol. 35, no. 24, 2008. [Online]. Available: https://agupubs.onlinelibrary.wiley.com/doi/abs/10.1029/2008GL036013

[93] E. R. Ojo, P. R. Bullock, J. L'Heureux, J. Powers, H. McNairn, and A. Pacheco, "Calibration and evaluation of a frequency domain reflectometry sensor for real-time soil moisture monitoring," *Vadose Zone Journal*, vol. 14, no. 3, p. vzj2014.08.0114, 2015. [Online]. Available: https://acsess.onlinelibrary.wiley.com/doi/abs/10.2136/vzj2014.08.0114

[94] G. L. Schaefer, M. H. Cosh, and T. J. Jackson, "The USDA natural resources conservation service soil climate analysis network (SCAN)," *Journal of Atmospheric and Oceanic Technology*, vol. 24, no. 12, pp. 2073–2077, 12 2007. [Online]. Available: http://journals.ametsoc.org/doi/10.1175/2007JTECHA930.1

[95] G. H. Leavesley, O. David, D. C. Garen, J. Lea, J. K. Marron, T. C. Pagano, T. R. Perkins, and M. L. Strobel, "A Modeling Framework for Improved Agricultural Water Supply Forecasting," in *AGU Fall Meeting Abstracts*, vol. 2008, Dec. 2008, pp. C21A–0497.

[96] M. Moghaddam, A. Silva, D. Clewley, R. AKBAR, S. Hussaini, J. Whitcomb, R. Devarakonda, R. Shrestha, R. Cook, G. Prakash, S. Santhana Vannan, and A. Boyer, "Soil moisture profiles and temperature data from soilscape sites, usa," 2016. [Online]. Available: http://daac.ornl.gov/cgi-bin/dsviewer.pl?ds_id=1339

[97] J. E. Bell, M. A. Palecki, C. B. Baker, W. G. Collins, J. H. Lawrimore, R. D. Leeper, M. E. Hall, J. Kochendorfer, T. P. Meyers, T. Wilson, and H. J. Diamond, "U.s. climate reference network soil moisture and temperature observations," *Journal of Hydrometeorology*, vol. 14, no. 3, pp. 977 – 988, 2013. [Online]. Available: https://journals.ametsoc.org/view/journals/hydr/14/3/jhm-d-12-0146_1.xml

[98] C. Mattar, A. Santamaría-Artigas, C. Durán-Alarcón, L. Olivera-Guerra, R. Fuster, and D. Borvarán, "The lab-net soil moisture network: Application to thermal remote sensing and surface energy balance," *Data*, vol. 1, no. 1, 2016. [Online]. Available: https://www.mdpi.com/2306-5729/1/1/6

Wolfgang Wagner (M'98–SM'07) received the Dipl.-Ing. degree in physics and the Dr.techn. degree in remote sensing from TU Wien, Austria, in 1995 and 1999 respectively. In support of his master and PhD studies he won fellowships to carry out research at NASA, ESA, and the EC Joint Research Centre. From 1999 to 2001 he was with DLR. In 2001 he was appointed professor for remote sensing at TU Wien. He is a co-founder of the EODC Earth Observation Data Centre. His main research interest is to gain physical understanding of the mechanisms driving the interaction of electromagnetic waves with the land surface. He has developed models for retrieving soil moisture and other land surface variables from scatterometer, SAR and full-waveform lidar observations. He is member of the advisory groups for METOP-SG SCA, Sentinel-1 NG and HydroGNSS. From 2008 to 2012 he served as ISPRS Commission VII President, from 2009 to 2011 as editor-in-chief of the Open Access Journal "Remote Sensing", and from 2016 to 2019 as chair of the GCOS/WCRP Terrestrial Observation Panel for Climate. He is a recipient of the ISPRS Frederick J. Doyle Award and the Friedrich Hopfner medal awarded by the Austrian Geodetic Commission.

Roland Lindorfer received the B.Sc. degree in Environmental Systems Sciences at KFU Graz, Austria, in 2019. Currently, he is pursuing his M.Sc. in Geodesy and Geoinformation at Vienna University of Technology (TU Wien), Austria, where he joined the Remote Sensing research group in 2020. In his research, Roland is interested in improving soil moisture retrievals from active microwave sensors with foci ranging from physical subsurface interactions to azimuthal backscatter dependencies.

Sebastian Hahn Sebastian Hahn received the B.Sc. degree in geodesy and geoinformatic engineering and the M.Sc. degree in geodesy and geophysics from the Vienna University of Technology (TU Wien), in 2009 and 2011, respectively. He is pursuing his Ph.D. degree in microwave remote sensing at TU Wien. He has been with the Department for Geodesy and Geoinformation at TU Wien since 2009 and is currently working as a Senior Scientist. His research interests include remote sensing over land using active microwave instruments, soil moisture retrieval algorithms and software engineering to develop remote sensing data services.

Hyunglok Kim Hyunglok Kim received his B.S. degree in civil and environmental engineering from Hanyang University, Seoul, South Korea, in 2012. He went on to obtain a master's degree in data science from the University of Virginia (UVA), Charlottesville, VA, USA, in 2021 and a Ph.D. degree in civil and environmental engineering from UVA in 2022. After completing his doctoral studies, he served as a postdoctoral research fellow at the United States Department of Agriculture (USDA)- Agricultural Research Service (ARS) Hydrology and Remote Sensing Laboratory from 2022 to 2023. In 2023, he transitioned to the Gwangju Institute of Science and Technology (GIST), located in the Republic of Korea, where he was appointed as an assistant professor at the School of Earth Sciences and Environmental Engineering. Throughout his career, Hyunglok's research interests have revolved around active and passive microwave remote sensing of soil moisture, land surface hydrology, data assimilation, and Bayesian machine learning. More recently, his focus has shifted towards applying Bayesian machine learning to remotely sensed and land surface model data for a better prediction of hydrometeorological variables. He was funded by NASA Earth and Space Science and Technology (FINESST 2019) for his project, "Diurnal Soil Moisture Using Satellite Observations and Data Assimilation." Additionally, in 2020, he was selected for the Robert E. Horton Fund for Hydrologic Research by the American Geophysical Union (AGU).

Mariette Vreugdenhil Mariette Vreugdenhil received her B.Sc. and M.Sc. in Earth Sciences from VU University Amsterdam, The Netherlands in 2009 and 2011. She obtained her Ph.D. in Remote Sensing from TU Wien, Vienna, Austria in 2016. She works as a Senior Scientist in the Remote Sensing Research Group at TU Wien. Her research focuses on the retrieval and analysis of vegetation and soil water content from Earth Observation data for numerous applications. In 2018 she was awarded a European Space Agency Living Planet Fellowship for her research on vegetation monitoring using Sentinel-1. Currently she focuses on drought monitoring and prediction using satellite soil moisture data.

Alexander Gruber Alexander Gruber received the M.Sc. degree in geodesy and geophysics and the Ph.D. degree in technical sciences from the Vienna University of Technology, Vienna, Austria, in 2013 and 2016, respectively. He is currently a Postdoctoral Researcher with the Climate and Environmental Remote Sensing Research Group, Department of Geodesy and Geoinformation, Vienna University of Technology. His research interests include land surface remote sensing, data assimilation, uncertainty characterization, and water and carbon cycle interactions.

Milan Fischer received his B.Sc. and M.Sc. in Soil Science at the Mendel University in Brno in 2006 and 2008. He received his Ph.D. in General Plant Production with dissertation work on the water balance of a short rotation culture in 2012. After that, he continued as a postdoctoral researcher at Global Change Research Institute (GCRI) of the Czech Academy of Sciences with the main focus on quantifying evapotranspiration using micrometeorological methods at ecosystem scale. Between 2014 and 2017 he spent a postdoc abroad in the lab of Dr. John King at North Carolina State University, USA. The main topic of this stay was an assessment of the loblolly pine and switchgrass intercropping system water balance. Since 2017, he has worked as a research assistant at GCRI and with the main focus on understanding plant-soil-atmosphere interactions at ecosystem up to continental scale, using in situ techniques, remote sensing, and hydrological modeling. He is also participating in national and global drought monitoring activities led by GCRI.

Miroslav Trnka received the M.Sc. degree (1999) in agroecology from Mendel University in Brno (MENDELU) and Ph.D. (2002) in Applied landscape ecology from MENDELU. In the same time he studied Law and Law Science at Masaryk´s University in Brno focusing on the Environmental law and air pollution regulation (graduated in 2001). All graduations were with distinction. He currently teaches climate and climate focused courses for agronomy, agroecology and forestry undergraduate and graduate students at the Faculty of Agronomy at MENDELU. He leads the Climate Analysis and Modeling Domain at Global Change Research Institute (GCRI) of the Czech Academy of Sciences, and he is research team leader focused on Agrosystem modeling and climate change impact analysis at GCRI. He has held a number of invited presentations at conferences and workshops in the USA, Austria, Germany, UK or France. Within Central Europe, he has been holding meetings with and for key stakeholders and decision makers, including hearings by two Prime Ministers of the Czech Republic, ministers and vice-ministers of Agriculture, ministers and vice-ministers of Environment, Senate and Lower House of the Czech Republic, the invited lecture for 27 ministers of agriculture in the Council of Ministers focusing on drought, and also potential impacts of climate change on Agriculture. Between 2016 and 2022 he has been leading the development of integrated strategies for climate change adaptation. In 2021 he was listed as the only Czech Scientist on the Thomson Reuters list of 1000 most influential Climate Scientists.

TABLE I
ANCILLARY DATA

Data set	Description	Source
Köppen-Geiger climate[+]	The Köppen-Geiger climate classification is divided into five main classes and 30 sub-types based on seasonality of monthly air temperature and precipitation. By this classification, complex climate gradients are aggregated into a simple but ecologically meaningful scheme. [67]	https://doi.org/10.6084/m9.figshare.6396959
Land cover[+]	The 300 m ESA CCI land cover classification is based upon the Medium Resolution Imaging Spectrometer archive as a basline and change detected from the Sentinel-3 OLCI time series for 2020. [68]	https://doi.org/10.24381/cds.006f2c9a
Soil groups[+]	SoilGrids™ maps available from the International Soil Reference and Information Centre (ISRIC) are a collection of soil property maps produced using machine learning at 250 m. The classification of most probable soil groups follows the World Reference Base. For more efficient processing, the 5-km-aggregated products were used for all datasets obtained from ISRIC. [69]	https://doi.org/10.17027/isric-soilgrids. c4dc161c-d62d-11ea-a1a3-292680b15169
Sand content[++]	The sand content, defined by particle sizes of 50/63-2000 μm in the surface layer (0-5 cm) and given in g kg^{-1}, was also extracted from SoilGrids. These predictions were derived using a digital soil mapping approach based on Quantile Random Forest, drawing on a global compilation of soil profile data and environmental layers.	https://doi.org/10.17027/isric-soilgrids. 713396fa-1687-11ea-a7c0-a0481ca9e724
Coarse fragments (CFVO)[++]	The 5-15 cm coarse fragment layer was extracted from the Soil-Grids250m 2.0 data base alike. It represents the volumetric content of fragments larger than 2 mm in the whole soil and is given in units of cm^{3}dm^{-3}. The depth of the layer chosen corresponds to the predicted penetration depth of C-band waves into dry soil.	https://doi.org/10.17027/isric-soilgrids. 713396f8-1687-11ea-a7c0-a0481ca9e724
Elevation [++]	Elevation (in meters) was extracted from the global 60 arc-second ETOPO 2022 global relief model resting on a combination of airborne lidar and satellite-derived topography information. The land topography data used in this study mainly originates from the Copernicus Digital Elevation Model (DEM) [70] as well as the Forest and Buildings Removed Copernicus DEM (FABDEM) [71] both provided at a 30 m grid. [72]	https://doi.org/10.25921/fd45-gt74
Leaf area index (LAI)[++]	A mean LAI map was created by averaging data from the Copernicus Global Land Service over snow free days from 2007 to 2020. The LAI is defined as half the total area of green elements of the canopy per unit horizontal ground area in units of m^2 m^{-2}. Practically, the LAI quantifies the thickness of the vegetation cover. [73]	https://land.copernicus.eu/global/products/lai
Lakes and wetlands[+]	The Global Lakes and Wetlands Database (GLWD) charts large lakes and reservoirs, smaller water bodies, rivers, and wetlands at a 30-second grid. GLWD proved to represent a comprehensive database of global lakes and to provide a good representation of the maximum global wetland extent in validations against documented data. [53]	https://www.worldwildlife.org/pages/ global-lakes-and-wetlands-database

[+] Categorical values were gridded to the 12.5 km fixed Earth grid used for ASCAT by selecting the dominant class within the ASCAT pixels.
[++] Continuous variables where gridded to the 12.5 km fixed Earth grid used for ASCAT by averaging values from the source grids over the ASCAT pixels.

TABLE II
NETWORKS AND NUMBER OF IN SITU STATIONS PER CONTINENT AFTER MASKING.

Network	Number	Reference
Africa		
AMMA-CATCH	7	Mougin et al. [74]
DAHRA	1	Tagesson et al. [75]
SD_DEM	1	Ardö [76]
TAHMO	4	van de Giesen et al. [77]
Australia		
OZNET	20	Smith et al. [78]
Europe		
FR_Aqui	4	Al-Yaari et al. [79]
HOAL	19	Blöschl et al. [80]
HOBE	30	Jensen and Refsgaard [81]
HYDROL-NET_PERUGIA	2	Flammini et al. [82]
IPE	1	Aldai et al. [83]
ORACLE	5	Riffard et al. [84]
REMEDHUS	22	González Zamora et al. [85]
RSMN	19	Ontel et al. [86]
SMOSMANIA	21	Calvet et al. [87]
TERENO	5	Bogena et al. [88]
UDC_SMOS	3	Schlenz et al. [89]
North America		
ARM	23	Cook 2016 [90]
FLUXNET-AMERIFLUX	2	Baldocchi et al. [91]
PBO_H2O	93	Larson et al. [92]
RISMA	9	Ojo et al. [93]
SCAN	154	Schaefer et al. [94]
SNOTEL	76	Leavesley et al. [95]
SOILSCAPE	80	Moghaddam et al. [96]
USCRN	86	Bell et al. [97]
South America		
LAB-net	1	Mattar et al. [98]

TABLE III

FRACTION OF PIXELS OR STATIONS, f_c IN %, FOR WHICH $\mathcal{P}_{ano}$, $\mathcal{P}_{sub}$ AND $\mathcal{S}_{sub}$ INDICATE THE OCCURRENCE OF SUBSURFACE SCATTERING WITHIN THE GIVEN CLIMATE, LAND COVER AND SOIL CLASSES. RESULTS ARE SHOWN FOR ERA5-LAND (E5L) WHEN THE NUMBER OF ASCAT PIXELS IS LARGER THAN 1000. FOR ISMN THE MINIMUM REQUIREMENT WAS 10 STATIONS PER CLASS. VALUES OF $f_c > 30$ % AND CORRESPONDING CLASSES ARE HIGHLIGHTED IN BOLD.

Class	Number of Pixels	Number of Stations	$\mathcal{P}_{ano}$ E5L	$\mathcal{P}_{ano}$ ISMN	$\mathcal{P}_{sub}$ E5L	$\mathcal{P}_{sub}$ ISMN	$\mathcal{S}_{sub}$ E5L	$\mathcal{S}_{sub}$ ISMN
Köppen-Geiger Climate Classification								
Af - Tropical, rainforest	2 220	–	2.5	–	4.1	–	2.2	–
Am - Tropical, monsoon	8 370	–	2.7	–	3.1	–	1.0	–
Aw - Tropical, savannah	79 959	–	4.7	–	1.2	–	0.5	–
BWh - Arid, desert, hot	133 615	26	**86.3**	**46.2**	**50.9**	**34.6**	**30.8**	**30.8**
BWk - Arid, desert, cold	37 745	41	**53.5**	**51.2**	**32.6**	**61.0**	16.2	**39.0**
BSh - Arid, steppe, hot	46 690	–	**38.7**	–	7.5	–	4.0	–
BSk - Arid, steppe, cold	42 889	181	24.0	**39.8**	12.8	**43.6**	5.5	15.5
Csa - Temperate, dry hot summer	6 450	94	**44.1**	9.6	25.9	20.2	9.9	17.0
Csb - Temperate, dry warm summer	3 427	15	24.6	20.0	14.4	21.4	5.7	13.3
Cwa - Temperate, dry winter, hot summer	22 395	–	14.4	–	8.9	–	6.3	–
Cwb - Temperate, dry winter, warm summer	8 954	–	2.9	–	4.6	–	2.8	–
Cfa - Temperate, no dry season, hot summer	27 647	185	0.4	2.2	7.3	21.6	4.7	7.0
Cfb - Temperate, no dry season, warm summer	8 981	67	2.0	7.5	11.2	**40.3**	8.0	25.4
Dsa - Cold, dry hot summer	1 416	–	**82.3**	–	**51.4**	–	27.5	–
Dsb - Cold, dry warm summer	1 867	24	**52.4**	**37.5**	**37.0**	**45.8**	22.9	8.3
Dwa - Cold, dry winter, hot summer	7 008	–	0.0	–	23.9	–	9.9	–
Dwb - Cold, dry winter, warm summer	4 001	–	0.0	–	20.7	–	16.5	–
Dfa - Cold, no dry season, hot summer	11 468	61	0.0	0.0	10.0	21.3	2.6	4.9
Dfb - Cold, no dry season, warm summer	29 518	146	0.3	6.8	12.3	**37.7**	8.4	26.0
Dfc - Cold, no dry season, cold summer	1 980	–	1.1	–	30.0	–	18.4	–
ESA CCI Land Cover Classification								
10 - Cropland, rainfed	50 219	47	12.3	6.4	5.3	17.0	2.4	8.5
11 - Cropland, rainfed, herbaceous cover	43 663	263	4.7	7.2	9.0	**33.5**	2.2	16.7
20 - Cropland, irrigated or post-flooding	12 280	–	27.9	–	26.1	–	10.2	–
30 - Mosaic cropland (>50%)/natural vegetation (<50%)	10 604	–	6.9	–	5.0	–	2.6	–
40 - Mosaic natural vegetation (>50%)/cropland (<50%)	8 785	13	10.0	10.0	6.5	7.7	3.2	0.0
50 - Tree cover, broadleaved, evergreen, closed to open (>15%)	15 542	–	1.9	–	8.3	–	6.7	–
60 - Tree cover, broadleaved deciduous, closed to open (>15%)	25 574	30	6.1	10.0	12.9	**36.7**	9.1	13.3
61 - Tree cover, broadleaved, deciduous, closed (>40%)	3 392	–	8.0	–	7.7	–	7.0	–
62 - Tree cover, broadleaved, deciduous, open (15-40%)	23 926	–	9.1	–	0.9	–	0.2	–
70 - Tree cover, needleleaved, evergreen, closed to open (>15%)	13 372	140	9.6	**32.1**	18.7	**48.6**	13.0	22.1
90 - Tree cover, mixed leaf type (broadleaved and needleleaved)	3 276	–	6.7	–	29.5	–	23.0	–
100 - Mosaic tree and shrub (>50%)/herbaceous cover (<50%)	8 222	–	21.5	–	12.6	–	7.7	–
110 - Mosaic herbaceous cover (>50%)/tree and shrub (<50%)	2 693	–	9.4	–	3.6	–	2.2	–
120 - Shrubland	58 124	129	**38.8**	**42.6**	13.8	**49.6**	7.5	27.9
122 - Deciduous shrubland	9 750	–	**32.8**	–	8.9	–	5.0	–
130 - Grassland	55 550	207	**31.5**	8.2	12.6	18.4	7.4	11.6
150 - Sparse vegetation (<15%)	31 211	–	**54.4**	–	16.7	–	8.5	–
153 - Sparse herbaceous cover (<15%)	1 482	–	**86.5**	–	**39.9**	–	25.7	–
190 - Urban areas	1 961	–	8.0	–	25.6	–	13.1	–
200 - Bare areas	106 304	–	**88.8**	–	**60.5**	–	**36.4**	–
ISRIC Soil Groups								
1-6 - Acrisols	46 127	45	4.5	0.0	3.8	13.3	2.2	0.0
7-9 - Albeluvisols	7 344	–	0.1	–	15.6	–	8.7	–
10-11 - Alisols	4 039	–	0.8	–	15.4	–	13.8	–
12-14 - Andosols	2 032	–	5.1	–	5.8	–	4.3	–
15-20 - Arenosols	85 611	11	**76.6**	**54.5**	**35.5**	0.0	16.1	9.1
21-24 - Calcisols	35 455	41	**63.7**	**46.3**	**35.9**	**51.2**	21.5	24.4
25-35 - Cambisols	43 205	127	**41.7**	11.0	15.5	**33.9**	9.4	19.7
36-38 - Chernozems	15 031	55	1.6	0.0	5.6	**36.4**	0.6	16.4
43-47 - Ferralsols	38560	–	2.9	–	1.0	–	0.4	–
48-52 - Fluvisols	7 432	–	20.3	–	25.3	–	12.4	–
53-58 - Gleysols	3 293	–	4.4	–	5.7	–	2.5	–
59-60 - Gypsisols	10 072	–	**84.8**	–	**63.4**	–	**42.8**	–
66-67 - Kastanozems	23 165	224	9.0	23.2	6.0	35.3	1.1	14.3
68-72 - Leptosols	44 915	19	**84.5**	**47.4**	**60.5**	**36.8**	**42.9**	15.8
73-75 - Lixisols	13 150	–	14.5	–	1.3	–	0.4	–
76-84 - Luvisols	50 083	217	20.5	12.4	11.6	**30.9**	6.8	15.7
85-86 - Nitisols	1 186	–	0.3	–	2.5	–	3.7	–
87-89 - Phaeozems	13 633	18	2.3	16.7	9.2	22.2	1.7	22.2
90-94 - Planosols	1 215	–	2.7	–	2.0	–	0.7	–
97-98 - Podzols	2 913	64	3.8	0.0	**39.0**	**35.9**	**35.9**	**31.3**
99-104 - Regosols	10 735	–	**73.7**	–	**46.4**	–	**30.8**	–
105-107 - Solonchaks	2 998	–	**68.0**	–	**39.7**	–	20.8	–
108-111 - Solonetz	5 479	–	13.1	–	9.2	–	2.5	–
115-118 - Vertisols	18 786	12	16.9	0.0	4.7	16.7	1.7	0.0

TABLE IV
RANK CORRELATIONS BETWEEN THE THREE INDICATORS $\mathcal{P}_{ano}$, $\mathcal{P}_{sub}$ AND $\mathcal{S}_{sub}$ AND SEVERAL LAND SURFACE VARIABLES. RESULTS ARE SHOWN USING ERA5-LAND (E5L) AND ISMN SOIL MOISTURE DATA AS INPUT.

Variable	$\mathcal{P}_{ano}$		$\mathcal{P}_{sub}$		$\mathcal{S}_{sub}$	
	E5L	ISMN	E5L	ISMN	E5L	ISMN
Soil moisture	–0.79	–0.48	–0.43	–0.04	–0.45	0.03
Leaf area index	–0.74	–0.43	–0.44	–0.16	–0.51	–0.11
Coarse fragments	0.55	0.55	0.44	0.22	0.47	0.23
Sand fraction	0.30	0.16	–0.00	0.05	–0.00	0.11
Elevation	0.24	0.41	0.13	0.22	0.07	0.10
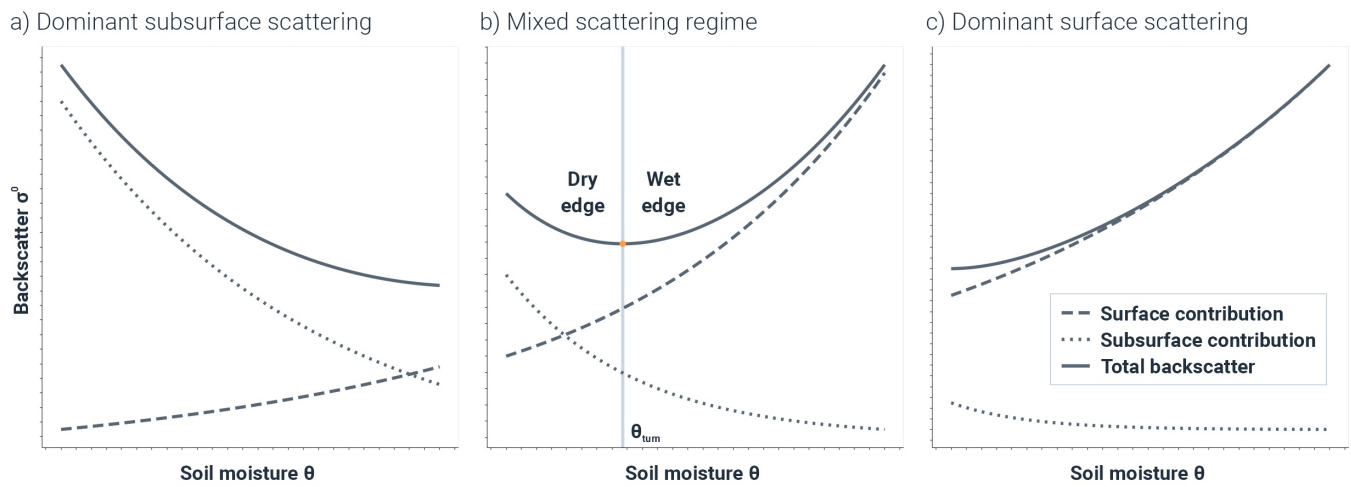
Fig. 1. Backscattering behavior of vegetation-covered soil with (a) dominant subsurface scattering, (b) mixed scattering, and (c) dominant surface scattering. Modified after [33].
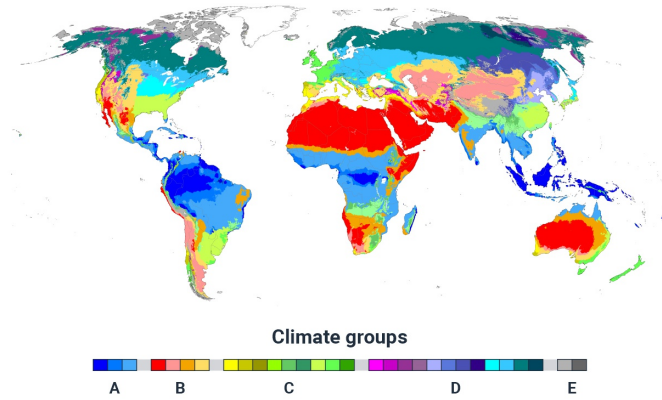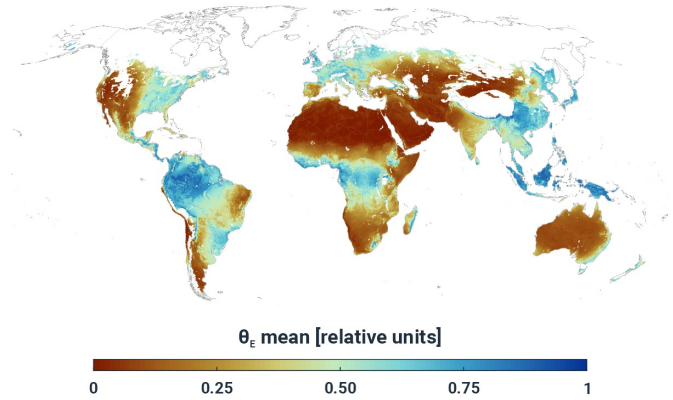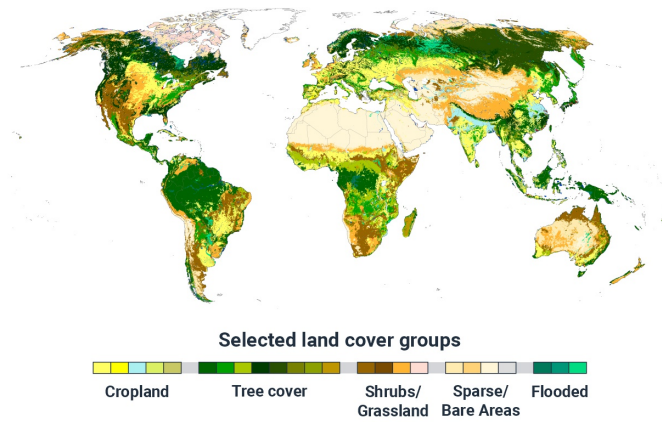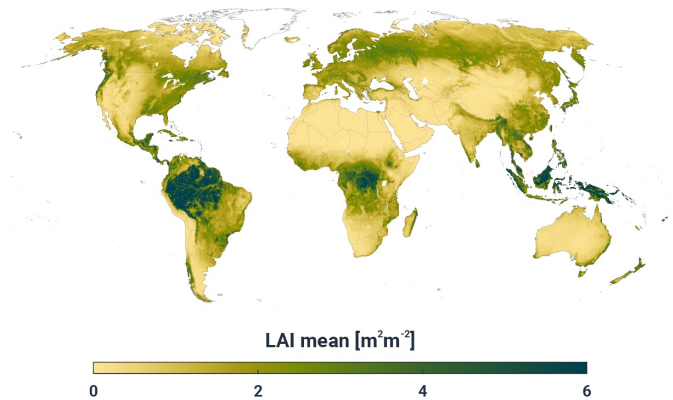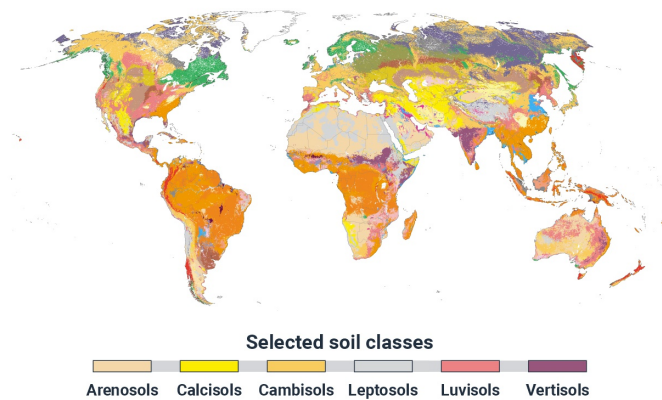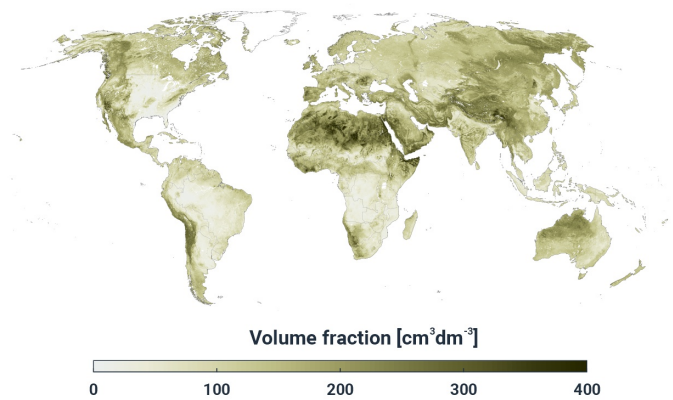
Fig. 2. Selected ancillary data sets for the analysis of the ASCAT backscatter data record and soil moisture retrievals: (a) Köppen-Geiger climate classification, (b) Mean ERA5-Land soil moisture over snow and frost-free days, (c) Land cover map from the ESA Climate Change Initiative (CCI), (d) Mean leaf area index (LAI) map from Copernicus Global Land Monitoring service (CGLS), (e) Soil groups from the International Soil Reference and Information Centre (ISRIC), (f) Volume fraction of coarse fragments in the 5–15 cm soil profile (CFVO) from ISRIC.
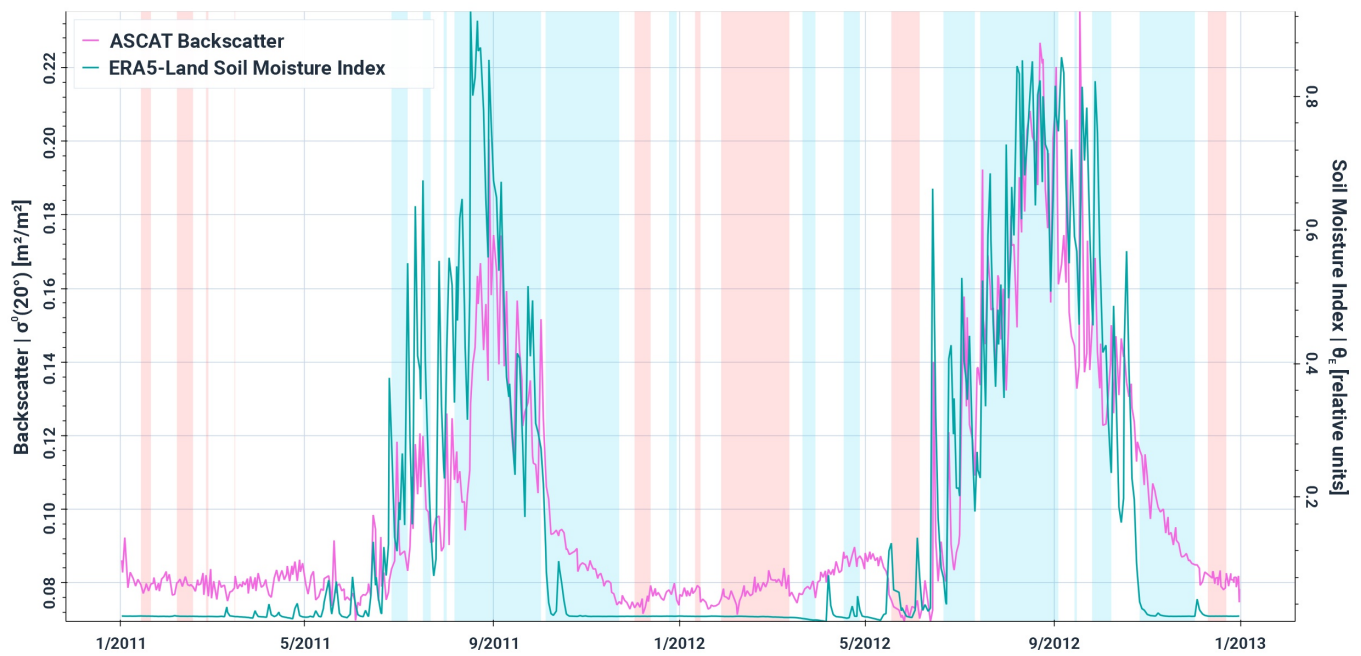
Fig. 3. Time series of ASCAT backscatter, $\sigma^0(20)$ in m^2 m^{-2}, and ERA5-Land soil moisture, θ_E in relative units, over the Sahel zone of Mali (14.128° N, 8.451° W) for the years 2011 and 2012. The light blue strips indicate where the short-term rank correlation ρ is higher than 0.4, and the light red strips that ρ is lower than -0.4.
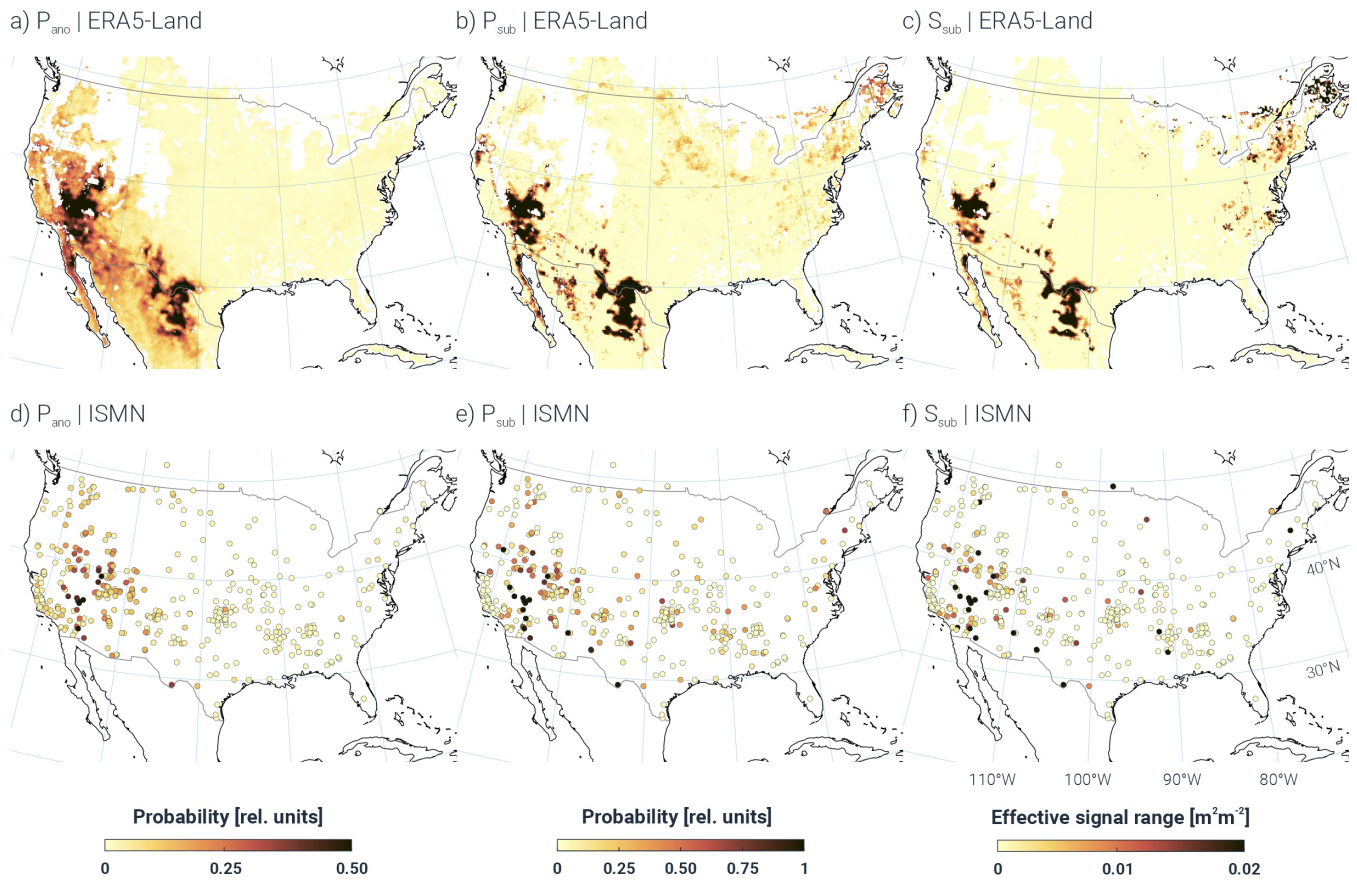
Fig. 4. Subsurface scattering indicators over the contiguous United States computed using ERA5-Land (top row) and ISMN (bottom row) soil moisture data as a reference.

a) P_{ano} | Probability of the occurrence of backscatter anomalies
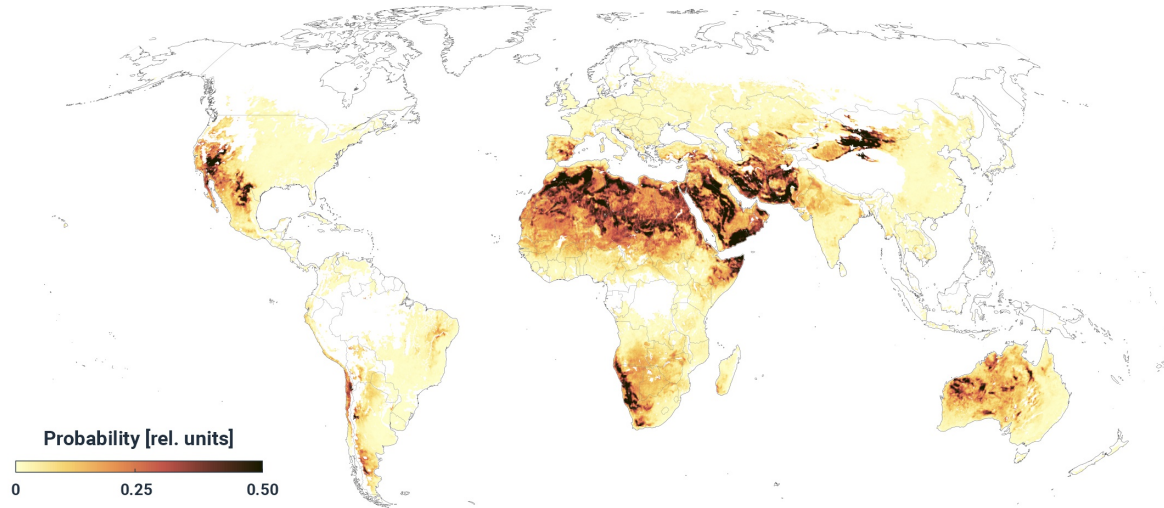
b) P_{sub} | Probability of detecting subsurface scattering
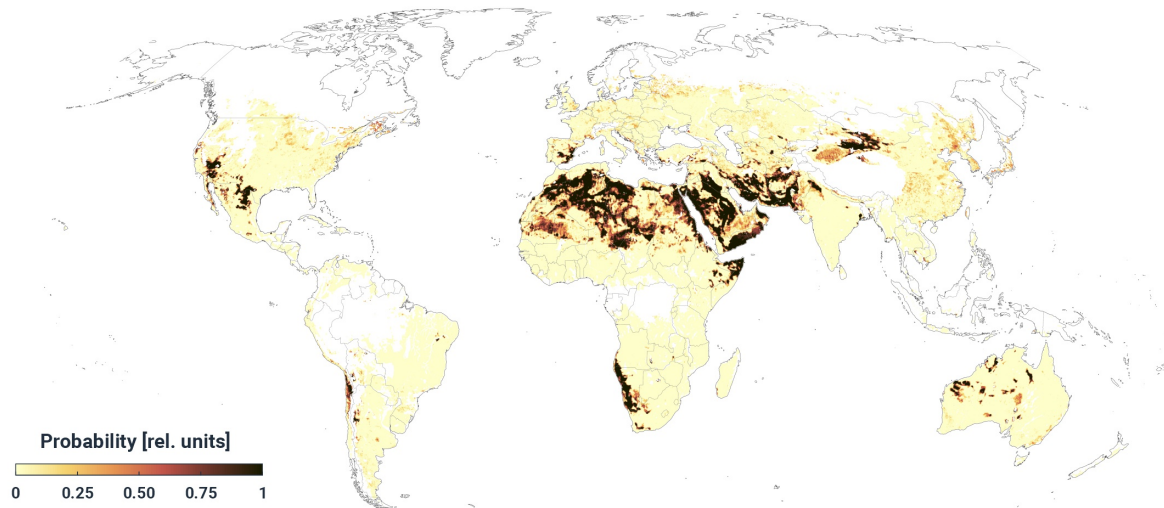
c) S_{sub} | Strength of the subsurface scattering signal
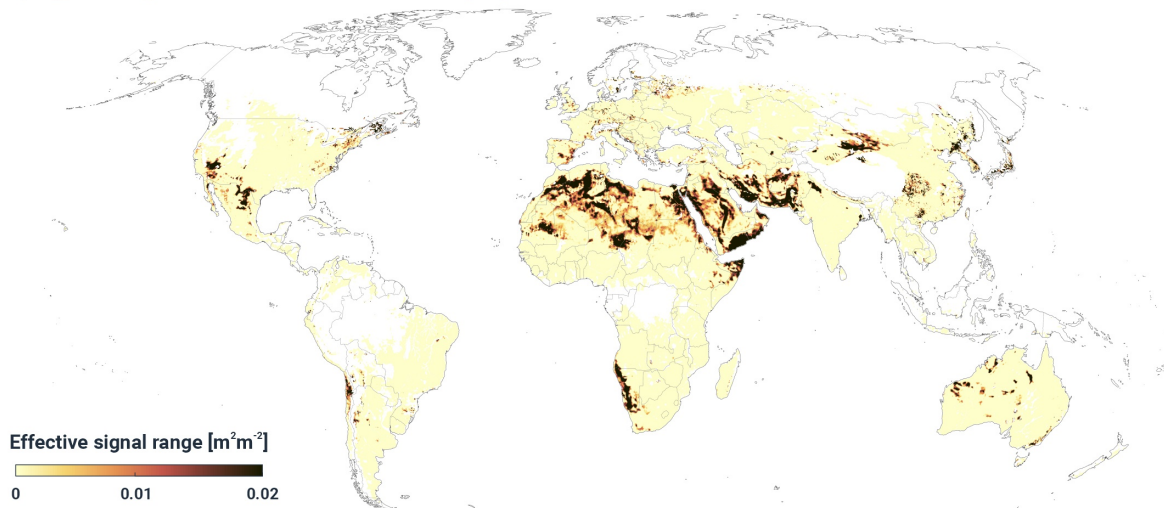
Fig. 5. Geographic distribution of subsurface scatterers as depicted by the three indicators: (a) probability of occurrence of backscatter anomalies, $\mathcal{P}_{ano}$, (b) probability of detecting subsurface scattering, $\mathcal{P}_{sub}$, and (c) subsurface scattering signal strength, $\mathcal{S}_{sub}$.
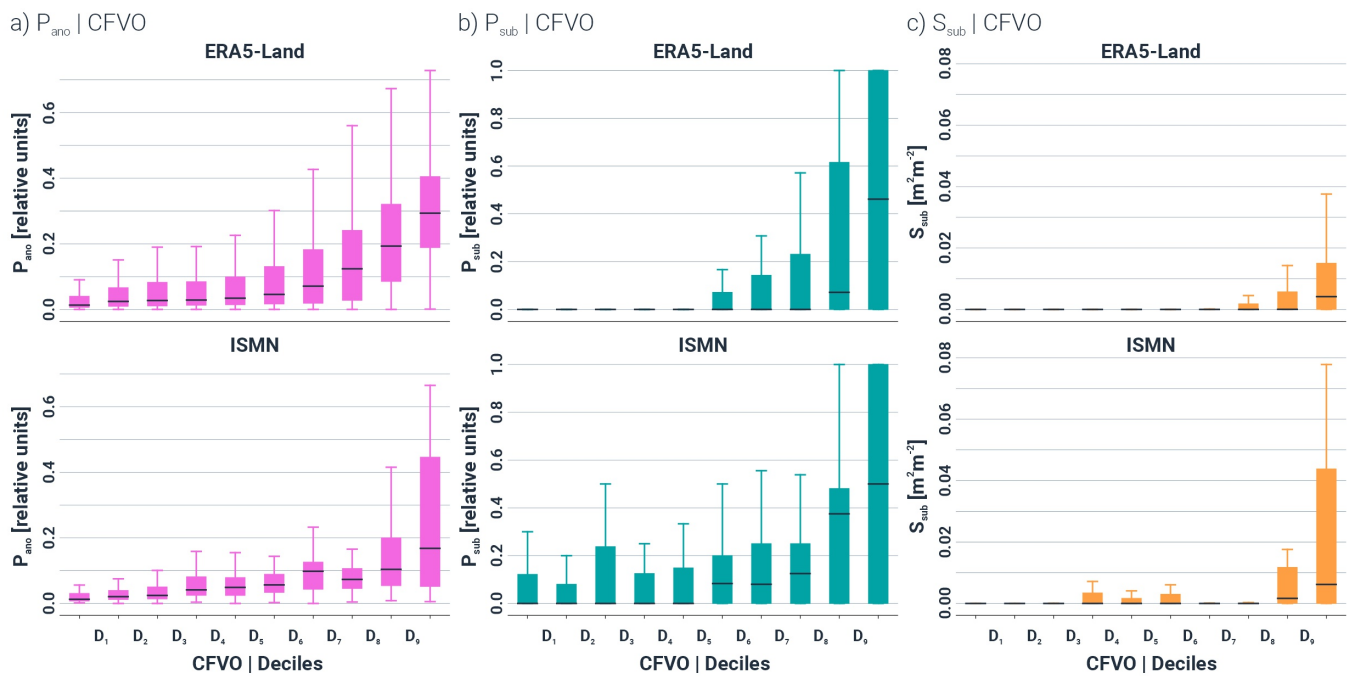
Fig. 6. Box plots of the three subsurface scattering indicators (a) $\mathcal{P}_{ano}$, (b) $\mathcal{P}_{sub}$ and (c) $\mathcal{S}_{sub}$ for an increasing number of coarse fragments in the 5–15 cm soil layer (separated in ten groups defined by the deciles of the worldwide CFVO histogram). The upper (lower) row shows the results using ERA5-Land (ISMN) soil moisture data as input for the calculation of the three indicators.
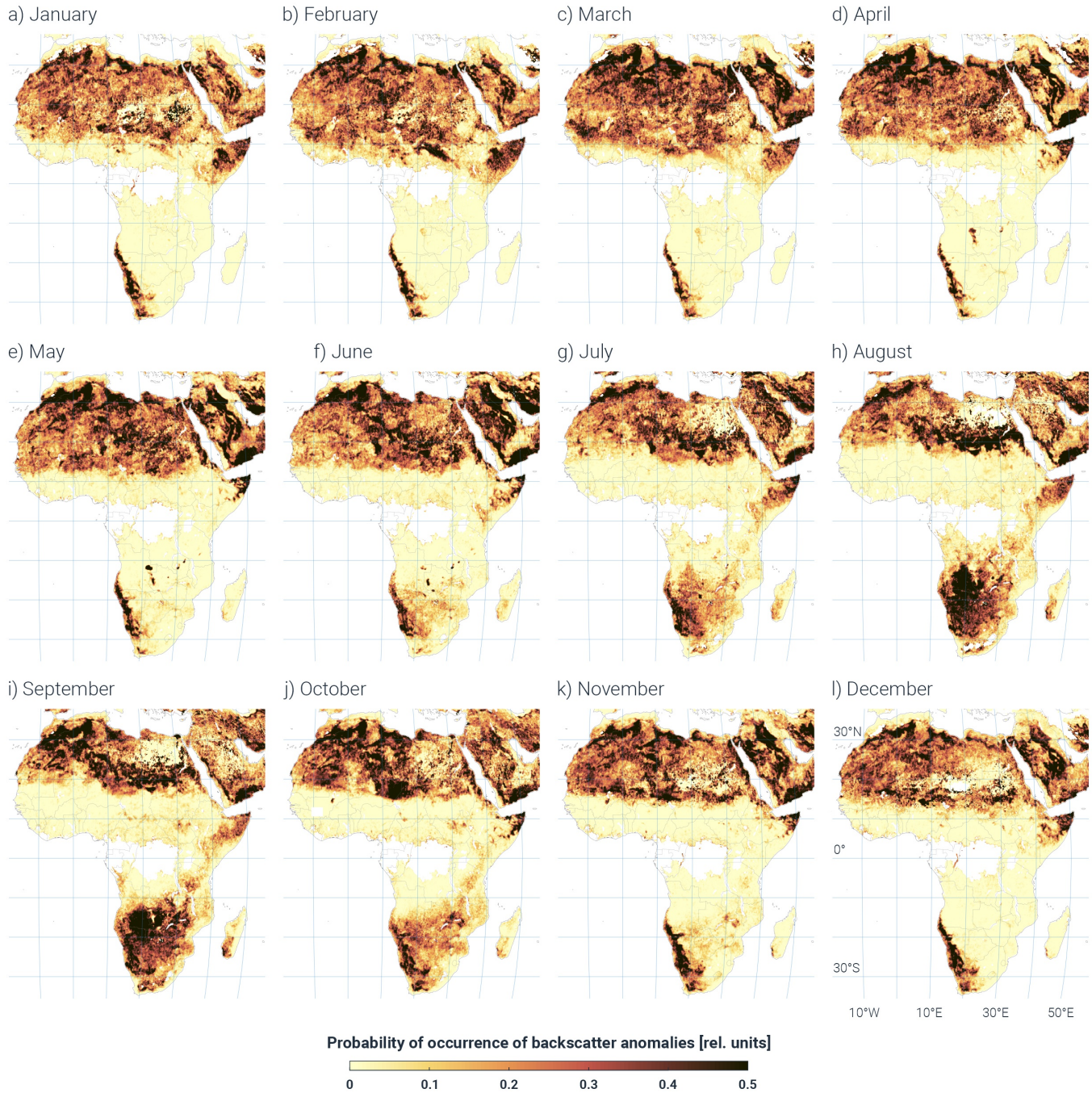
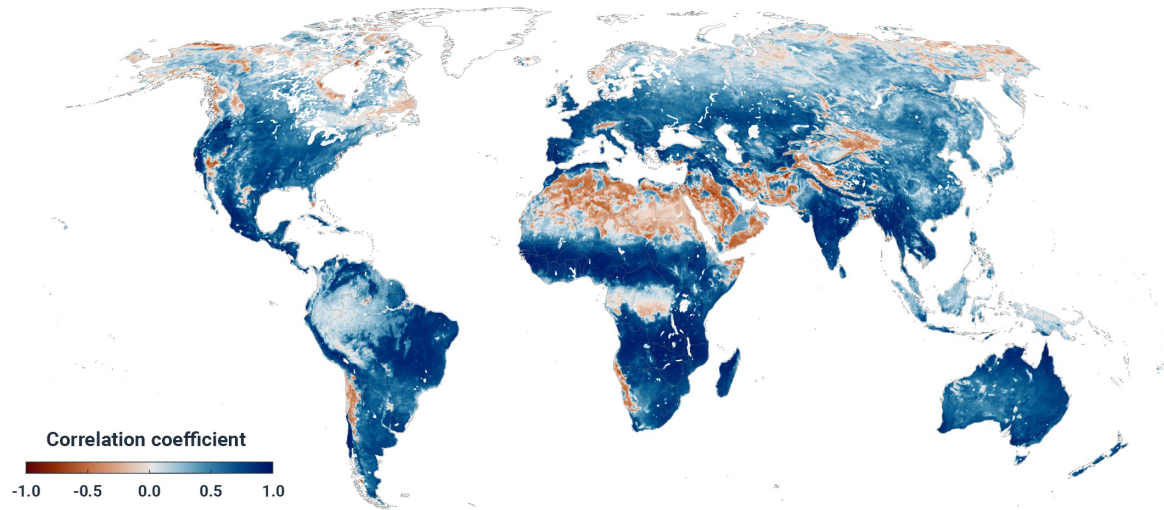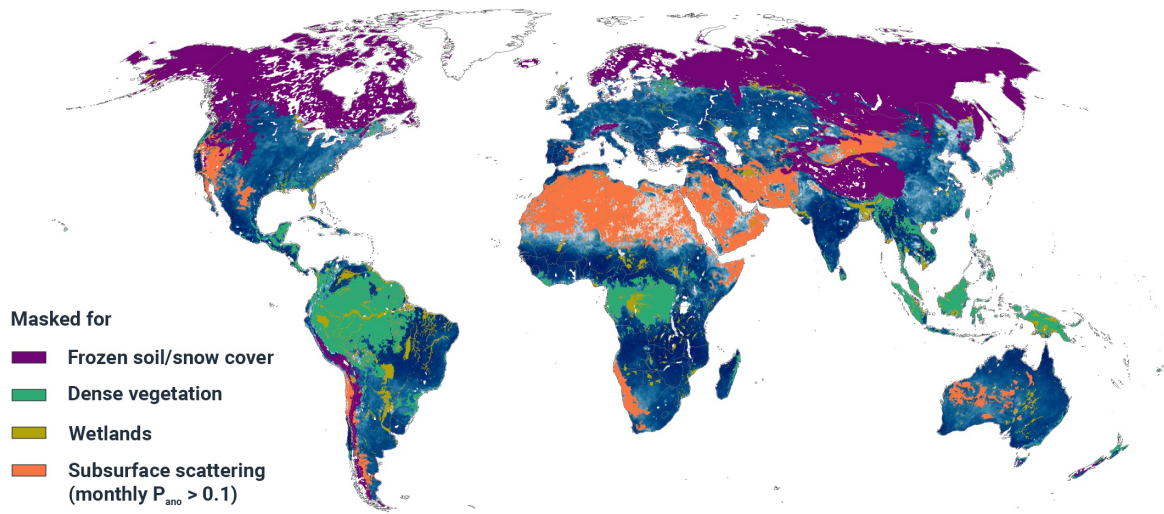Fig. 7. Seasonality of the occurrence of backscatter anomalies $\mathcal{P}_{ano}$ over Africa.

a) Pearson correlation coefficient R between ASCAT SSM and ERA5-Land SM

b) R with masks applied

Fig. 8. Pearson correlation R between ASCAT SSM and ERA5-Land soil moisture data for the years 2007 to 2021 without masking (top) and after applying masks for frozen soil/snow cover, dense vegetation, wetlands, and subsurface scattering, masking months with $\mathcal{P}_{ano} > 0.1$ (bottom).
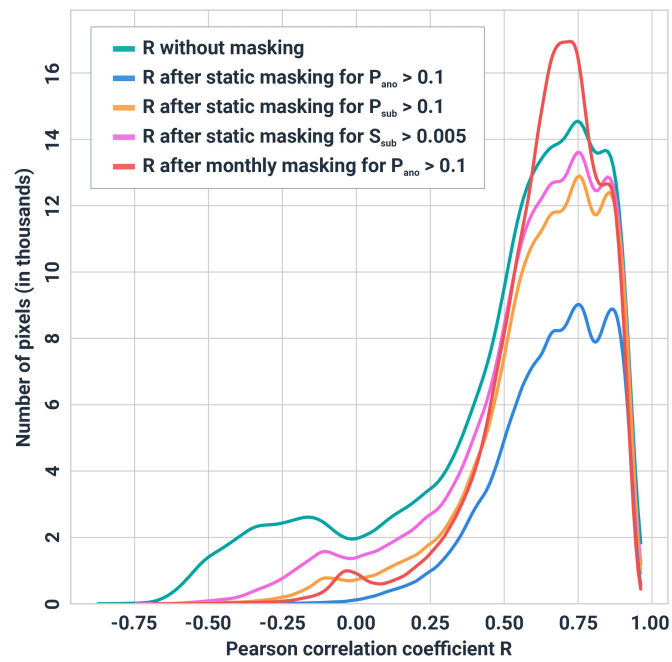
Fig. 9. Smoothed histograms of the Pearson correlation R between ASCAT SSM and ERA5-Land soil moisture data for different subsurface scattering masking criteria: no mask, $\mathcal{P}_{ano} > 0.1$, $\mathcal{P}_{sub} > 0.1$, $\mathcal{S}_{sub} > 0.005$ m^2 m^{-2}, and monthly $\mathcal{P}_{ano} > 0.1$. The smoothed lines are based on 100 histogram bins per distribution of R.